JNeurosci
THE JOURNAL OF NEUROSCIENCE

Research Articles: Development/Plasticity/Repair

Long-term neuroinflammation induced by influenza A virus infection and the impact on hippocampal neuron morphology and function

Shirin Hosseini[1,2], Esther Wilk[3], Kristin Michaelsen-Preusse[1], Ingo Gerhauser[4], Wolfgang Baumgärtner[4], Robert Geffers[5], Klaus Schughart[3,6,7] and Martin Korte[1,2]

[1]*Department of Cellular Neurobiology, Zoological Institute, TU Braunschweig, Germany*
[2]*Helmholtz Centre for Infection Research, Neuroinflammation and Neurodegeneration Group, Braunschweig, Germany*
[3]*Helmholtz Centre for Infection Research, Department of Infection Genetics, Braunschweig, Germany*
[4]*Department of Pathology, University of Veterinary Medicine Hannover, Germany*
[5]*Helmholtz Centre for Infection Research, Genome Analytics Research Group, Braunschweig, Germany*
[6]*Department of Infection Genetics, University of Veterinary Medicine Hannover, Germany*
[7]*Department of Microbiology, Immunology and Biochemistry, University of Tennessee Health Science Center, Memphis, TN, USA*

DOI: 10.1523/JNEUROSCI.1740-17.2018

Received: 22 June 2017

Revised: 12 January 2018

Accepted: 19 January 2018

Published: 26 February 2018

Author contributions: S.H. performed research; S.H., E.W., and K.M.-P. analyzed data; E.W., K.S., and M.K. designed research; K.M.-P., K.S., and M.K. wrote the paper; I.G., W.B., and R.G. contributed unpublished reagents/analytic tools.

Conflict of Interest: The authors declare no competing financial interests.

We thank Christin Kurch for excellent technical assistance and Marta Zagrebelsky and Ab Osterhaus for comments on the paper. This study was in part supported by the Niedersachsen-Research Network on Neuroinfectiology (N-RENNT) of the Ministry of Science and Culture of Lower Saxony (to K.S. and M.K.), the SFB854 (to M.K.), and intra-mural grants from the Helmholtz-Association (Program Infection and Immunity) (to KS).

Corresponding Author: Martin Korte, PhD, E-Mail: m.korte@tu-bs.de, Phone: +49 (0) 531 3913220, Fax: +49 (0) 531 3913222, TU Braunschweig, Germany, Zoological Institute, Div. Cellular Neurobiology, Spielmannstr 7, 38106 Braunschweig, Germany

Cite as: J. Neurosci ; 10.1523/JNEUROSCI.1740-17.2018

Long-term neuroinflammation induced by influenza A virus infection and the impact on hippocampal neuron morphology and function

Shirin Hosseini[1,2*], Esther Wilk[3*], Kristin Michaelsen-Preusse[1*], Ingo Gerhauser[4], Wolfgang Baumgärtner[4], Robert Geffers[5], Klaus Schughart[3,6,7*], Martin Korte[1,2*#]

[1] Department of Cellular Neurobiology, Zoological Institute, TU Braunschweig, Germany
[2] Helmholtz Centre for Infection Research, Neuroinflammation and Neurodegeneration Group, Braunschweig, Germany
[3] Helmholtz Centre for Infection Research, Department of Infection Genetics, Braunschweig, Germany
[4] Department of Pathology, University of Veterinary Medicine Hannover, Germany
[5] Helmholtz Centre for Infection Research, Genome Analytics Research Group, Braunschweig, Germany
[6] Department of Infection Genetics, University of Veterinary Medicine Hannover, Germany
[7] Department of Microbiology, Immunology and Biochemistry, University of Tennessee Health Science Center, Memphis, TN, USA
[*] equal contribution

[#] Corresponding Author:

Martin Korte, PhD
E-Mail: m.korte@tu-bs.de
Phone: +49 (0) 531 3913220
Fax: +49 (0) 531 3913222
TU Braunschweig, Germany
Zoological Institute, Div. Cellular Neurobiology
Spielmannstr 7
38106 Braunschweig
Germany

Numbers of pages: 40 pages
Number of figures: 10 figures
Number of tables: 1 table
Abstract: 250 words
Introduction: 619 words
Discussion: 1493 words

Abbreviated title: Long-term neuroinflammation induced by IAV infection

Conflict of interest: The authors declare no competing financial interests.

Acknowledgement
We thank Christin Kurch for excellent technical assistance and Marta Zagrebelsky and Ab Osterhaus for comments on the paper. This study was in part supported by the Niedersachsen-Research Network on Neuroinfectiology (N-RENNT) of the Ministry of Science and Culture of Lower Saxony (to K.S. and M.K.), the SFB854 (to M.K.), and intra-mural grants from the Helmholtz-Association (Program Infection and Immunity) (to KS).

Abstract

Acute influenza infection has been reported to be associated with neurological symptoms. However, the long-term consequences for the CNS of an infection with neurotropic but also with non-neurotropic influenza A virus (IAV) variants remain elusive. We can show that spine loss in the hippocampus after infection with neurotropic H7N7 (rSC35M) as well as non-neurotropic H3N2 (maHK68) in female C57BL/6 mice persists well beyond the acute phase of the disease. While spine number was significantly reduced 30 days post infection (pi) with H7N7 or H3N2, full recovery could only be observed much later at 120 days pi. Notably, infection with H1N1 virus which was shown previously to acutely affect spine number and hippocampus-dependent learning had no significant long-term effects. Spine loss was associated with an increase in the number of activated microglia, reduced long-term potentiation in the hippocampus, and an impairment in spatial memory formation indicating that IAV associated inflammation induced functional and structural alterations in hippocampal networks. Transcriptome analyses revealed regulation of many inflammatory as well as neuron- and glia-specific genes in H3N2 and H7N7 infected mice at day 18 and in H7N7 infected mice at day 30 pi that related to the structural and functional alterations. Our data provide evidence that neuroinflammation induced by neurotropic H7N7 and infection of the lung with a non-neurotropic H3N2 IAV result in long-term impairments in the CNS. IAV infection in humans may therefore not only lead to short-term responses in infected organs but also trigger neuroinflammation and associated chronic alterations in the CNS.

Keywords: dendritic spines, structural plasticity, hippocampus, influenza, neuroinflammation

Significance statement

In the acute phase of influenza infection, neuroinflammation can lead to alterations in hippocampal neuronal morphology as well as cognitive deficits. The results of this study now also provide evidence that neuroinflammation induced by IAV infection can induce longer lasting virus-specific alterations in neuronal connectivity detectable still one month after infection which are associated with impairments in spatial memory formation. IAV infection in humans may therefore not only lead to short-term responses in infected organs but also trigger neuroinflammation and associated chronic alterations in the CNS.

Introduction

Influenza is a highly contagious disease caused by RNA viruses affecting birds and mammals, with a high risk of serious illness and death worldwide. While the primary target of influenza viruses in mammals is the lung, neurological complications were also reported (Ekstrand, 2012; Shah et al., 2014). However, the mechanisms and consequences of neuroinflammation caused by influenza A viruses (IAV) are only partly understood. Neurotropic IAV strains are indeed able to enter the central nervous system (CNS) through the blood-brain barrier or microvascular endothelial cells (Tomonaga, 2004). For instance, the highly pathogenic avian influenza virus (H5N1) can infect the CNS and subsequently lead to neuronal cell death in the substantia nigra pars compacta (Kristensson, 2006; Jang et al., 2012) induced by neuroinflammation through the activation of glial cells and altered pro-inflammatory/inflammatory cytokine expression (Jang et al., 2009; Jang et al., 2012). Interestingly, neuropsychiatric complications were not only reported after infection with neurotropic IAV variants but also after non-neurotropic H1N1 virus infection, especially in children (Surana et al., 2011). Neurodevelopmental problems were shown to be a risk factor for a severe outcome following influenza infection including death in children (CDC, 2012; Ekstrand, 2012). In this scenario activation of the peripheral innate immune system can induce the production of pro-inflammatory/inflammatory cytokines such as interleukin-1β (IL-1β), IL-6 and tumor necrosis factor-α (TNF-α) within the brain (Thomson et al., 2014; Riazi et al., 2015), thereby severely affecting cognition and emotional behavior (Raison et al., 2006; Camara et al., 2015).

The hippocampus, a brain region involved in learning and memory processes (Korte and Schmitz, 2016) is especially sensitive to neuroinflammation (Vitkovic et al., 2000; Lynch, 2002; Heneka et al., 2014). Inflammatory cytokines can impair hippocampal long-term potentiation (LTP) (Pickering and O'Connor, 2007; Riazi et al., 2015) and inhibit neurotrophic factor signaling thereby negatively influencing synaptic plasticity and memory formation (Tong et al., 2008; Tong et al., 2012). Furthermore, a decrease in hippocampal dendritic spine density and impairment in synaptic plasticity could be observed following activation of peripheral as well as central immune responses (Jurgens et al., 2012; Vasek et al., 2016). Indeed, it is now well established that a peripheral immune stimulation can affect the intact CNS (Richwine

et al., 2008) via the activation of microglia during a secondary, mirror inflammatory response in the brain (Riazi et al., 2015). Microglia, CNS-resident macrophages, are usually the first to be activated in response to brain infections or damage. In contrast to this non-activated or ‘‘resting’’ microglia perform housekeeping functions within the healthy CNS including synapse turnover and synaptic plasticity. Thus, long-term microglial activation might interfere with these processes (Nimmerjahn et al., 2005; Yirmiya and Goshen, 2011; Hristovska and Pascual, 2015).

Whereas a short-term influence of IAV infection on hippocampal neuron morphology and cognition was recently shown in mice for non-neurotropic PR8 (H1N1) IAV (Jurgens et al., 2012), long-term effects have not been studied so far. Here, we investigated the impact of three different IAV variants on hippocampal neuron morphology and hippocampus-dependent behavior. First, we used the well-characterized PR8 (A/PuertoRico/8/34) non-neurotropic virus (Majde et al., 2007; Hodgson et al., 2012). The second non-neurotropic virus belonged to the H3N2 subtype, maHK68 (mouse-adapted A/Hong-Kong/1/68) (Haller et al., 1979). As a model for neurotropic IAV infection, the polybasic rSC35M (recombinant A/Seal/Mass/1/80 mouse-adapted, H7N7) was used (Gabriel et al., 2005). The long-term consequences of infections with these viruses on CNS function and morphology have not been investigated in detail.

Here, we describe impairments in spatial learning associated with alterations in hippocampal structure and function as well as an increased number of activated microglia as long-term consequences of IAV infection. These findings point towards long-term hippocampal neuroinflammation as the cause of the neurological symptoms that lasted for one month after the infection.

Materials and Methods

Ethics statement. The experiments performed with mice were approved according to the animal welfare law in Germany. All protocols used in this project have been reviewed and approved by the local committees at the Helmholtz Centre for Infection Research and TU Braunschweig and the authorities (LAVES, Oldenburg, Germany; permit number: 3392 42502-04-13/1234) according to the national guidelines of the animal welfare law in Germany (‘Tierschutzgesetz in der Fassung der Bekanntmachung vom 18. Mai 2006 (BGBl. I S. 1206, 1313), das zuletzt durch Artikel 20 des Gesetzes vom 9. Dezember 2010 (BGBl. I S. 1934) geändert worden

ist.'). The virus was prepared by infection of 10-day-old embryonated chicken eggs obtained from a commercial vendor (Charles River Germany).

Viruses and mice. Stocks of viruses were obtained from Stefan Ludwig, University of Münster (PR8M, A/PuertoRico/8/34 (H1N1)), Münster variant (Blazejewska et al., 2011), Georg Kochs, University of Freiburg (maHK68, mouse-adapted A/Hong-Kong/1/68 (H3N2)) (Haller et al., 1979), and from Gülsah Gabriel, Heinrich-Pette Institute, Hamburg (rSC35M, mouse-adapted A/Seal/Mass/1/80 (H7N7)) (Gabriel et al., 2005). Virus stocks were propagated by infection of 10-day-old embryonated chicken eggs (PR8M, maHK68) or in MDCK (Madin-Darby Canine Kidney) cell culture (rSC35M) as described previously (Wilk and Schughart, 2012). Female inbred mice of the strain C57BL/6J were obtained from Janvier, France and maintained under specific pathogen-free conditions, according to the German animal welfare law.

Mouse infections. Female C57BL/6J mice (Janvier, France) at the age of 8-10 weeks were anaesthetized by intraperitoneal injection of 0.9% (w/v) NaCl (Merck) ketamine-xylazine solution (85% NaCl (0.9%), 10% ketamine (100 mg/ml), 5% xylazine (20 mg/ml); 10 ml per 1 kg body weight) and then infected intranasally with a dose of 10 (H3N2 and H7N7) or 2×10^3 (H1N1) FFU (Focus Forming Units) of the respective virus in 20 µl sterile phosphate-buffered saline (PBS). Body weight was monitored for two weeks after infection. Mice showing more than 30% of body weight loss were euthanized.

Viral load in the brain. To detect low amounts of virus in brain of infected mice, egg infection was used as a more sensitive method to determine viral load. For this purpose brains were homogenized in PBS with 0.1% bovine serum albumin (BSA) using the Fast Prep® instrument. Debris was removed by centrifugation for 10 min at 1000 rpm. The samples were stored in aliquots at -70 °C. In a first test, 50 µl of undiluted samples were given per embryonated egg (3 replicates per sample). After 48 h incubation at 37 °C, allantoic fluid was harvested and tested using the haemagglutination assay (Wilk and Schughart, 2012) for virus positivity. Samples identified to be positive for the virus were further quantified by the 50% egg infectious dose assay as described by (Szretter et al., 2006). Titers were calculated using the Reed-Muench method.

Histology. Brains from infected mice on indicated days after infection were extracted in *toto* and immersion-fixed for 24-72 h in 4% buffered formaldehyde solution (pH 7.4). After fixation and before embedding the brains were separated in transverse sections using a coronal matrix system following the standard guidelines (Morawietz et al., 2004). In addition to the recommended planes, the nasal part was divided within the sagittal median to include the olfactory bulbs in the histological analysis. Sections of brains (0.5 µm) were cut with the microtome and stained with hematoxylin and eosin (H&E) or immune-stained with mouse-anti-Influenza A virus nucleoprotein (NP), Clone Hb65, mouse IgG2a (Kerafast, Cat# FCG013, RRID:AB_2716646). Inflammation in the infected brain was evaluated using a semi-quantitative scoring system for perivascular mononuclear cuffing (0 = normal, + = single inflammatory cells, ++ = 2-3 layers of infiltrates, +++ = more than 3 layers of infiltrates). In addition, immunohistochemistry for the virus was analyzed by using a semi-quantitative scoring system from 0 = no, 1 = few, 2 = multiple, 3 = numerous infected cells (Gerhauser et al., 2007). Several brain regions (olfactory bulb, cerebral cortex, corpus striatum/basal ganglia, thalamus/hypothalamus, hippocampus, mesencephalon, cerebellum, medulla oblongata) were evaluated separately and a mean value determined for each animal.

Behavioral assays. For behavioral evaluation, four groups of 8-10 weeks old female C57BL/6J mice were treated intranasally with PBS as control, H1N1, H3N2 and H7N7 influenza A virus strains, then were assigned to two different time points of the experiment including 30 and 120 days post infection (n=7-10). All behavioral experiments were performed the same time of day during the light period by a blind experimenter to all types of treatment groups.

Open field test. In order to investigate influenza-induced illness behavior and willingness of the mice to explore, the open field test was performed as previously described (Walsh and Cummins, 1976). Briefly, mice were placed along one side of a white PVC open field apparatus (40 cm × 40 cm × 40 cm) for 5 min. The central area of the arena was specified as the center part (30 cm × 30 cm). Between each session of experiments, the apparatus was cleaned with Bacillol®. Movement data including total distance traveled, average speed and percentage of activity in the periphery and in the center part of the arena were collected by ANY-maze behavioral tracking software (Stoelting, Dublin, Ireland, RRID:SCR_014289).

Elevated plus maze test. In order to investigate influenza-induced anxiety-like behavior, the elevated plus maze test was performed as previously described (Hogg, 1996). In this test, the apparatus is comprised of a cross with two opposed open arms (25 cm × 5 cm) and two opposed closed arms (25 cm × 5 cm, surrounded by 20 cm high walls). The arena was made of white PVC and was elevated 50 cm above the floor. Mice were placed in the central part of the arena (5 cm × 5 cm) facing toward an open arm and permitted to move freely in the arena for 5 min. Locomotion data including the percentage of time spent in open and closed arms were collected by ANY-maze behavioral tracking software (Stoelting, Dublin, Ireland, RRID:SCR_014289).

Morris water maze test. In order to investigate the effects of influenza A virus infection on cognitive function, spatial learning and memory formation were assessed using the initial training and the reversal learning phase of the Morris water maze paradigm (Morris, 1984; Vorhees and Williams, 2006). The maze is comprised of a circular pool 150 cm in diameter and 19-20 ^{o}C water temperature. The platform was 10 cm in diameter and hidden 1 cm underneath the surface of the opaque water (Titaandioxide, Euro OTC Pharma). Prior to the training a visible platform task was performed as a pre-training and was used to ensure that swimming ability and visual acuity were intact in control and treated animals. During this phase, the animals had two trials (maximum of 60 s each) per day for three consecutive days to reach the visible platform, the position was altered during the trials (data are not shown). Subsequently, training in the Morris water maze test was performed for 8 days with the invisible platform located in the northeast (NE) quadrant. Each day, animals were placed in the water for four trials, with different starting points (SE, S, W, and NW) randomly. The animals were permitted to swim freely for 60 s or until the platform was reached. Otherwise, they were guided to the platform and allowed to sit on it for 20 s. A detailed analysis of the swimming path allows for a qualitative assessment of learning in mice. Progressively over time, healthy animals switch from egocentric (hippocampus-independent: chaining, scanning and random swimming) to allocentric (hippocampus-dependent: directed search) strategies to navigate to the hidden platform while a spatial map of the maze is formed (Garthe et al., 2009; Garthe and Kempermann, 2013). The pathway map to find the platform was analyzed as follows: searching strategies including scanning characterized by <60% and >10% surface

coverage, chaining characterized by >80% time in a doughnut-shaped annulus zone and random swimming characterized by >60% surface coverage of the whole pool area, directed search characterized by >80% time in Wishaw's corridor (Whishaw, 2004; Garthe et al., 2009; Garthe and Kempermann, 2013).

To evaluate memory retrieval, two probe trial tests were performed at the third and at the sixth day of the acquisition training, prior to starting the four trials of training at that day. Another reference memory test was performed 24 h after the last day of acquisition training. During the probe trial, the platform was removed and the animals were allowed to swim freely for 45 s. After the third probe trial test, the platform was moved to the opposite quadrant of the pool (SW) to test the ability of the animals to form a new memory. The task consisted of three training days. On the fourth day, one single probe trial was performed (D'Hooge and De Deyn, 2001). All data including the escape latency (time to reach the platform), percentage of searching time spent in the four quadrants of the pool, percentage time spent in the border (thigmotaxis), annulus (chaining), central circle (scanning) zones and Whishaw's corridor (directed search) of the pool, and occupancy plots of the presence in the quadrants for the animals groups were collected by ANY-maze behavioral tracking software (Stoelting, Dublin, Ireland, RRID:SCR_014289).

Electrophysiological experiments. To investigate the function of CA1 hippocampal neurons, electrophysiological recording experiments were performed at 30 and 120 days post infection. At 30 days post infection, a total number of 45 and at 120 days post infection, 38 acute hippocampal slices were prepared from fourteen and twelve female mice in three groups which were inoculated by PBS as control and H3N2 and H7N7 influenza virus, 8-10 weeks after birth. Briefly, mice were deeply anesthetized with 100% CO_2 then sacrificed and brains were quickly removed and transferred into ice-cold carbogenated (95% O_2 and 5% CO_2) artificial cerebrospinal fluid (ACSF) containing: 124 mM NaCl, 4.9 mM KCl, 1.2 mM KH_2PO_4, 2.0 mM $MgSO_4$, 2.0 mM $CaCl_2$, 24.6 mM $NaHCO_3$ and 10 mM D-glucose at pH=7.4. Afterwards, the hippocampus was dissected and transverse hippocampal slices (400 µm) were obtained by using a manual tissue chopper (whole procedure was done in 2–3 min). The hippocampal slices were transferred to an interface recording chamber (Scientific System Design), where they were incubated at 32 °C with a constant flow rate (0.5 ml/min) of carbogenated ACSF for 2 hours prior to the start of recordings.

Field excitatory postsynaptic potentials (fEPSPs) were recorded in the *stratum radiatum* of the CA1 region in hippocampal slices. Responses were evoked by stimulation of the Schaffer collateral pathway using two monopolar, lacquer coated stainless-steel electrodes (5 MΩ; AM Systems). These stimulation electrodes (S1 and S2) were positioned equidistantly on both sides of the recording electrode and by this means two independent stimulation pathways could be used for the same CA1 recordings region. For recording fEPSPs (measured as the first slope function), the recording electrode (5 MΩ; AM Systems) was placed in the CA1 apical dendritic layer (at least 20 µm away from the *stratum pyramidale*) and signals were amplified by a differential amplifier (Model 1700, AM Systems). The signals were digitized using a CED 1401 analog-to-digital converter (Cambridge Electronic Design). An input-output curve (afferent stimulation vs. fEPSP slope) for assessment of basal synaptic transmission was generated after the pre-incubation period. Test stimulation intensity was modified to be adjusted to extract fEPSP slope as 40% of the maximal fEPSP response for both synaptic inputs S1 and S2. To investigate short-term plasticity, a paired-pulse stimulation protocol was used with two consecutive stimuli with equal intensity from one of the stimulating electrodes in each hippocampal slice. Paired-pulse facilitation (PPF) could be extracted from the fEPSP slopes as a response to the second stimulation over the first one at different interpulse intervals of 10, 20, 40, 60, 80, and 100 ms. To investigate long-term potentiation, 20 min after baseline recording, LTP was induced by Theta-burst stimulation (TBS) including four bursts at 100 Hz repeated 10 times in a 200 ms interval. This stimulation was repeated three times in a 10 seconds interval. Only healthy sections with a stable baseline were included in the electrophysiological data analysis. The slope of fEPSPs was measured over time and normalized to the baseline. Data acquisition and off-line analysis were performed using IntraCell software (Version 1.5, LIN, Magdeburg, 2000).

Golgi-Cox staining. To investigate the long-term effects of influenza A virus infection on hippocampal neuron morphology, four groups of 2 months old female C57BL/6J mice were inoculated intranasally with PBS as control, H1N1, H3N2 and H7N7 influenza A virus strains. Mice were deeply anaesthetized with CO_2 and sacrificed via decapitation at 30, 60 and 120 days post infection (N = 4-5). The whole brain was removed rapidly. The left hemisphere was prepared for further

immunohistochemical experiments whereas the right one was incubated in FD rapid Golgi stain kit (FD NeuroTechnologies, Inc., Columbia, USA) according to the manufacturer's protocol. Afterwards, hemispheres were blocked in 2% agar and 200 µm thick coronal sections were cut with a vibratome (Leica VT 1000 S) and mounted on gelatin-coated glass slides. Subsequently, the sections were processed for signal development before being dehydrated through graded alcohols and mounted using Permount (Thermo Fisher Scientific).

Immunohistochemistry. To determine the inflammatory response in the hippocampus following influenza infection, the left hemisphere was isolated and fixed in 4% paraformaldehyde (PFA) for 24 hours and then cryoprotected in 30% sucrose solution in 0.1 M phosphate buffer (PB) for 24 hours and stored in Tissue-Tek® O.C.T.™ compound (A.Hartenstein Laborversand) at -70 ºC. For fluorescence immunostaining, 30 µm sections were cut using a freezing microtome (Frigomobil, R.Jung Heidelberg, Germany). Afterwards, ten successive sections (five for IBA-1 staining and five for GFAP staining) were washed with PBS 1X and blocked in PBS 1X solution containing 0.2% Triton X-100, 10% goat serum and 1% BSA for 1 hour at room temperature. Sections were incubated overnight at 4 ºC with the following primary antibodies: anti-ionized calcium-binding adaptor molecule 1 (IBA-1) (1:1000; rabbit polyclonal, Synaptic Systems, Cat# 234 003, RRID:AB_10641962) and anti-glial fibrillary acidic protein (GFAP) (1:1000; mouse monoclonal, Sigma-Aldrich, Cat# G3893, RRID:AB_477010) were diluted in PBS 1X, 0.2% Triton X-100 and 10% goat serum. Secondary antibodies were Cy™3-conjugated AffiPure Goat Anti-Rabbit IgG (H+L) (1:500; Jackson ImmunoResearch Labs, Cat# 111-165-144, RRID:AB_2338006) and Cy™3-conjugated AffiPure Goat Anti-Mouse IgG (H+L) (1:500; Jackson ImmunoResearch Labs, Cat# 115-165-068, RRID:AB_2338686) which were diluted in PBS 1X. Sections were mounted using Fluoro-gel mounting medium (Electron Microscopy Sciences, Hatfield, PA).

Imaging and image analysis. To survey the hippocampal neuron morphology, second- or third-order branches of apical dendrites within the CA1 and CA3 as well as dendrites within the dentate gyrus (DG) superior and inferior subregions of the hippocampus (10 cells per animal, 40-50 dendrites per group) were imaged in three-dimensions (z-stack thickness of 0.5 µm) using an Axioplan 2 imaging microscope (Zeiss) equipped with an ApoTome module (Zeiss) with a 63X (N.A. 1) oil objective

accompanied with a digital camera (AxioCam MRm, Zeiss). In all selected neurons, spine density per micrometer dendrite was calculated using Fiji software (BioVoxxel, RRID:SCR_015825) on the segments of dendritic branches with a length of more than 60-70 µm which were located at least 50 µm away from the soma. The total number of spines along the segments of dendritic branches was counted manually by an investigator blinded to the type of treatment.

The IBA-1- and GFAP-stained images from hippocampal subregions including CA1, CA3, superior and inferior blade of DG (N=2-5 mice per each group and 5 frame per each animal, 10-25 frame per each group) were taken in three-dimensions (z-stack thickness of 1 µm) using an Axioplan 2 imaging microscope (Zeiss) microscope equipped with a 20X objective (N.A. 0.8) and a digital camera (AxioCam MRm, Zeiss). To quantify the density of microglia and astrocytes, a region of interest (ROI) was drawn in each frame of the hippocampal subregions and the total number of IBA-1 and GFAP positive cells with clearly visible nuclei by DAPI were counted manually by Fiji software (BioVoxxel, RRID:SCR_015825) and the sampled volume was calculated. Results are expressed as the number of cells per mm^3 tissues and then normalized to control. For morphometric analysis of IBA-1 positive cells, at least 30 microglial cells (6 cells per each ROI) were randomly selected per hippocampal subregions of IBA-1 stained images from each animal (N = 4-5 per group, 120-200 microglial cells per each group). The total primary microglial cell processes were counted using Fiji software (BioVoxxel, RRID:SCR_015825). For the immunohistochemical experiments, all slides were coded and analysis was performed blindly.

Evaluation of blood-brain barrier permeability. To determine the blood-brain barrier (BBB) integrity following influenza A virus infection, spectrophotometry was used. 8 weeks old female C57BL/6J mice (N = 3-4 per each group) were infected by H3N2 and H7N7 influenza A virus, then at 4, 8 and 10 days post infection they were injected with a 2% Evans blue solution (Sigma-Aldrich) in normal saline (4 ml/kg of body weight) intraperitoneally. The dye was allowed to distribute by the circulatory system for 5 hours (4 and 8 days post infection) to 20 hours (10 days post infection). Afterwards, the mice were sacrificed and the brain was isolated and frozen in liquid nitrogen and stored at −70°C until further use. The preparation of tissue for assessing the presence of Evans blue stain in the brain as an indicator of a compromised BBB

was performed as described previously (Manaenko et al., 2011). Evans blue absorbance was detected at 610 nm using a spectrophotometer (Denovix DS-11 fx, USA).

Enzyme-linked immune sorbent assay (ELISA). To quantify the presence of proinflammatory cytokines including IFN-γ and TNF-α in the blood serum and the supernatant of homogenized hippocampi or brain hemispheres of influenza infected mice, ELISA experiment was performed. For this purpose, 8 weeks old female C57BL/6J mice (N = 3-4 per each group) were inoculated with influenza A virus strains and PBS as a control. Body weight was monitored and the samples were collected at 8 days post infection (before, the maximum body weight loss was observed at this time). Mice were deeply anaesthetized with CO_2 and sacrificed via decapitation. Blood was collected using a pipette and incubated for at least 30 minutes at room temperature. To separate the serum from the cellular blood components, the samples were centrifuged at 2000 g for 20 min at room temperature. The supernatant was immediately frozen in liquid nitrogen. For protein isolation, the tissue was homogenized using an Eppendorf-fitting pestle in 400 µl STKM lysis buffer (250 mM Sucrose, 50 mM Tris-HCl, 25 mM KCl and 5 mM $MgCl_2$) containing a protease inhibitor cocktail (cOmplete™). The samples were centrifuged for 10 min at 4 °C at 13000 g. The supernatant was collected and stored at -70 °C. To determine cytokine level, a mouse IFN-γ and TNF-α ELISA kits (R&D System, MN, USA) were used according to the manufacturer's recommendations. Absorbance at 450 nm was measured with a Tecan Sunrise™- microplate reader with a wavelength correction at 680 nm connected to Magellan software. Finally, the measured optical density of the reaction was compared with the optical density of the known standard samples to determine protein concentration in the samples.

RNA isolation and gene expression analysis by microarray. On days 18 and 30 post infection mice were euthanized by CO_2 asphyxiation and the hippocampus was removed. Immediately after dissection, the tissue was placed into RNAlater solution (Qiagen), incubated overnight at 4 °C and stored at -20 °C. For each group, hippocampi from at least three mice were prepared as independent biological replicates. Tissues were homogenized with FastPrep®-24 instrument placing them in a 2 ml lysing matrix tube (MP Biomedicals) containing 1 ml QIAzol Lysis Reagent. Homogenization was performed with 6.0 m/s speed for 1 min. Isolation of RNA was

performed with the Rneasy Lipid Tissue Mini Kit (Qiagen). The quality and integrity of the RNA was controlled on the 2100 Bioanalyzer (Agilent Technologies). For DNA microarray hybridization, 100 ng of total RNA was applied for the Cy3-labelling reaction using the one color Quick Amp Labeling protocol (Agilent Technologies). Labeled cRNA was hybridized to Agilent´s mouse 4x44k microarrays for 16 h at 68 °C and scanned using the Agilent DNA Microarray Scanner.

Microarray data were analyzed using the R software package (R_Core_Team, 2013a) (R Project for Statistical Computing, RRID:SCR_001905). Pre-processing steps included background correction, quantile normalization and annotation using the MmAgilentDesign026655.db (Carlson, 2014), LIMMA (Smyth, 2004), and Agi4x44PreProcess (Gentleman et al., 2004) packages. Multi-group comparisons and identification of differentially expressed probesets (DEPs) were performed with the LIMMA package (Smyth, 2004) using Benjamini-Hochberg correction for multiple testing (Benjamini and Hochberg, 1995). DEPs between two groups were identified based on an adjusted p-value of < 0.1 and exhibiting more than a 1.4-fold ($\log_2$ of 0.5) difference in expression levels. KEGG pathway enrichment analysis and cluster profiling was performed with the package clusterProfiler (Yu et al., 2012). The raw data has been deposited in the GEO expression database (http://www.ncbi.nlm.nih.gov/geo/) under the accession number GSE106620.

Experimental design and statistical analyses. All experimental design are explained in the respective parts of materials and methods section. Data were analyzed and plotted by GraphPad Prism 6 (GraphPad Software, RRID:SCR_002798) and presented as mean±SEM. Statistical analysis for each experiment are indicated in the result section and figure legends, including number of animals (N), number of brain slices, cells and samples, statistical test used (one-way and two-way ANOVA and repeated measure ANOVA or unpaired two-tailed t-test) as well as post hoc analysis (Bonferroni's and Benjamini-Hochberg test). Unless specified otherwise the minimum significance value was considered as $p < 0.05$. All experiments were analyzed in a strictly blind fashion.

Results

Infection of C57BL/6J mice with different influenza A virus (IAV) variants - establishing mouse models to study the long-term effects of influenza infection on CNS function

Female C57BL/6J mice at the age of 8-10 weeks were infected with influenza A viruses (IAV) by intranasal instillation with three different mouse-adapted viruses. Earlier studies demonstrated that female mice are more susceptible and produce more neutralizing antibodies and higher levels of chemokines and cytokines than males during infection with influenza viruses (Geurs et al., 2012). Therefore, only female mice were used in this study. Here, we investigated three different IAV. We chose the well characterized non-neurotropic mouse-adapted human PR8 (H1N1) virus (Blazejewska et al., 2011) which is known to enter the olfactory nerves and the glomerular layer of the olfactory bulb (OB) within 4 hours after intranasal infection but without further replicating in the brain or inducing neuropathology (Majde et al., 2007; Hodgson et al., 2012). This specific IAV variant was also used by Jurgens et al. demonstrating altered hippocampal neuron morphology and impaired cognition during the acute phase of the infection (7 days post infection) (Jurgens et al., 2012). In addition, we included another non-neurotropic mouse-adapted human IAV strain, the maHK68 (H3N2) (Haller et al., 1979) in our studies for which we established a well-characterized mouse model (Leist et al., 2016). Furthermore, we included the neurotropic virus rSC35M (H7N7) which was isolated from seals and adapted to mouse (Gabriel et al., 2005). The advantage of using this virus is that most infected mice survive the infection. This allowed us to study the long-term effects of a neurological IAV infection. Such studies cannot be performed with the highly pathogenic H5N1 virus that is often used as model for neurotropic IAV infections because all infected mice will die within 5-10 days post infection (pi). Avian H7N7 viruses are able to infect humans and represent a potential future pandemic threat (Lang et al., 1981; Banks et al., 1998; Fouchier et al., 2004; Shinya et al., 2005).

The infection doses for all three viruses were adjusted to sub-lethal concentrations allowing us to study long-term effects of IAV infections. Using these doses, 100% of H1N1 (100 ± 0 %, N = 37), 84% of H3N2 (84.12 ± 4.60 %, N = 63) and 76% of H7N7 (76.34 ± 4.40 %, N = 93) infected mice survived the infection. The infection with all three viruses resulted in comparable body weight losses (Fig. 1A). The maximum weight loss in H3N2 (N = 13) and H7N7 infected mice (N = 18) occurred at day 9 pi and in H1N1 infected animals (N = 11) at day 8 pi.

First, the brains of IAV infected mice were analyzed for the presence of infectious virus particles (Fig. 1B). For this, we used the highly sensitive egg-infectious dose assay. In line with previous publications, we did not detect any infectious virus particles in the brains of H1N1 infected mice, whereas infectious particles were found in different regions of the brain (mesencephalon, thalamus, medulla oblongata, cerebellum, cortex, olfactory bulb and hippocampus) after H7N7 infection. In the brain of H3N2 infected mice no or only very low amounts of infectious virus particles could be detected confirming that it is not able to efficiently replicate in the CNS (Fig. 1B).

To investigate in detail the pathological alterations caused by infections with the three viruses, histological sections of the brain were analyzed. In the brain of H7N7 infected mice many cells stained positive for viral NP (nuclear protein). Also moderate infiltration of meningeal and perivascular immune cells (B-cell, T-cell and macrophages) and several foci of gliosis (astrocytes and microglia) were detected (Fig. 1C-F). However, no lesions and only few single NP positive cells were observed following H3N2 infection (Fig. 1C, E-F). In the case of H1N1, we did not observe any pathological changes. Additional analysis of other organs by PCR and immunohistochemistry verified that H3N2 was detectable but did not replicate in other organs than the lung.

IAV infection causes cognitive impairment

As influenza infection can be accompanied by neurological symptoms (Ekstrand, 2012) we were interested whether the infection with different virus strains would affect mouse behavior in a virus-specific manner. We chose the well-established Morris water maze task as a paradigm to investigate the long-term consequences of an IAV infection influence on learning and spatial memory formation (Morris, 1984; Vorhees and Williams, 2006). Prior to the learning paradigm, general locomotor activity and exploratory behavior were tested in the open field test to exclude that phenotypes observed in the water maze task would be purely attributable to hyperactivity in infected individuals. Neither control nor IAV infected mice did show any sickness behavior or deficits in locomotors activity (Fig. 2A-D). On the other hand, the outcome of the Morris water maze task can be influenced by anxiety, for instance, when the animals avoid the open water part of the maze and rather show thigmotaxis behavior staying close to the pool walls. We, therefore, tested for a

potential increase in anxiety-related behavior 30 and 120 days pi using the elevated plus maze test. Control, as well as infected mice, did not reveal significantly elevated anxiety levels (Fig. 2E-F).

To investigate the effects of IAV infection on cognitive function, training in the Morris water maze task was performed starting at 30 and 120 days pi (Fig. 3-5). During 8 days of acquisition training, the escape latency reduced significantly in control, as well as in infected mice (Fig. 3A-B), thereby indicating that all groups showed hippocampus-dependent spatial learning and memory formation (Repeated measure one-way ANOVA: $F_{Ctrl\text{-}30dpi}$ (7, 49) = 11.21, p = 0.000 (N = 8), $F_{H1N1\text{-}30dpi}$ (7, 63) = 12.99, p = 0.000 (N = 10), $F_{H3N2\text{-}30dpi}$ (7, 42) = 9.50, p = 0.000 (N = 7), $F_{H7N7\text{-}30dapi}$ (7, 49) = 7.19, p = 0.000 (N = 8), $F_{Ctrl\text{-}120dpi}$ (7, 42) = 18.11, p = 0.000 (N = 7), $F_{H3N2\text{-}120dpi}$ (7, 42) = 5.61, p = 0.000 (N = 7) and $F_{H7N7\text{-}120dpi}$ (7, 49) = 10.11, p = 0.000 (N = 8)). Yet, the escape latency in H7N7 infected mice 30 days pi was significantly increased compared to control, non-neurotropic H1N1 and H3N2 IAV infected mice (Fig. 3A), pointing out an impairment in memory formation following infection with this neurotropic virus (two-way ANOVA $F_{treatment}$ (3, 1024) = 57.85, p < 0.0001 (both factors fixed)). Three months later, at day 120 pi analysis of the escape latency in control as well as IAV infected mice during the training did not reveal any significant differences (Two-way ANOVA $F_{treatment}$ (2, 680) = 0.35, p = 0.70 (both factors fixed), Fig. 3B). To assess memory retrieval, reference memory tests (probe trials) were performed at day 3, 6 and 9 of the training phase (Fig. 3C-D). The results revealed that the percentage of time spent in the target quadrant by H1N1 and H3N2 IAV infected mice at day 30 pi increased over the training time similar to control mice (One-way ANOVA: $F_{Day\ 3}$ (2, 22) = 2.48, p = 0.10, $F_{Day\ 6}$ (2, 22) = 1.04, p = 0.37 and $F_{Day\ 9}$ (2, 22) = 3.23, p = 0.058). H7N7 infected mice showed an impairment in memory retrieval indicated by a significantly reduced preference for the target quadrant on day 6 and 9 compared to the other groups tested (One-way ANOVA: $F_{Day\ 3}$ (3, 29) = 3.22, p = 0.03, $F_{Day\ 6}$ (3, 29) = 5.78, p = 0.003 and $F_{Day\ 9}$ (3, 29) = 3.91, p = 0.01, Fig. 3C). At 120 days pi the quadrant preference was comparable between all groups irrespective of the previous infection ($F_{Day\ 3}$ (2, 19) = 0.27, p = 0.76, $F_{Day\ 6}$ (2, 19) = 1.38, p = 0.274, $F_{Day\ 9}$ (2, 19) = 0.20, p = 0.81, Fig. 3D).

A detailed analysis of the swimming path allows for a qualitative assessment of learning in mice (Fig. 4). All groups of control and IAV infected mice showed an augmentation of hippocampus-dependent searching during the training. However,

this progression was clearly decreased for H3N2 and H7N7 IAV infected animals 30 days pi (Day 4: Ctrl: 40.62 ± 8.09 %, H1N1: 42.50 ± 8.37 %, H3N2: 21.42 ± 6.52 % and H7N7: 18.75 ± 4.09 %) (Two-way ANOVA $F_{treatment}$ (3, 232) = 11.29, $p < 0.0001$ (both factors fixed), Fig. 4A). No significant differences in the relative percentage of strategies used between IAV infected and control mice were observed during the training 120 days pi (Two-way ANOVA $F_{treatment}$ (2, 152) = 1.32, $p = 0.26$ (both factors fixed), Fig. 4B).

In the reversal Morris water maze paradigm which is dependent on cognitive flexibility, the hidden platform was moved to the opposite quadrant (SW) (Fig. 5). During 3 days of training, the escape latency to the new platform position decreased significantly in control (Repeated measure one-way ANOVA: $F_{Ctrl\text{-}30dpi\text{-}R}$ (2, 14) = 16.15, $p = 0.000$), H1N1 ($F_{H1N1\text{-}30dpi\text{-}R}$ (2, 18) = 42.28, $p = 0.000$) and H7N7 ($F_{H7N7\text{-}30dpi\text{-}R}$ (2, 14) = 8.75, $p = 0.003$) influenza infected mice but not in H3N2 IAV infected mice at 30 days pi ($F_{H3N2\text{-}30dpi\text{-}R}$ (2, 12) = 2.59, $p = 0.08$, Fig. 5A). H7N7 IAV infected mice showed a significantly increased escape latency compared to control and H1N1 infected mice. Therefore, both H3N2 and H7N7 viruses led to a reduced ability to memorize the new location of the hidden platform 30 days pi (Two-way ANOVA $F_{treatment}$ (3, 384) = 9.30, $p < 0.0001$ (both factors fixed), Fig. 5A). IAV infected mice tested 120 days pi revealed no significant differences in escape latency compared to control animals (Two-way ANOVA $F_{treatment}$ (2, 255) = 2.85, $p = 0.059$ (both factors fixed), Fig. 5B). Subsequently, a single probe trial test 24 hours after the last day of reversal training was performed (Fig. 5C-D). 30 days pi, both control and H1N1 infected mice spent significantly more time in the new target quadrant (T) in comparison with the average time spent in non-target quadrants (Ctrl: unpaired t test $p < 0.0001$, df = 30 and H1N1: Unpaired t test $p < 0.0001$, df = 38) whereas H3N2 (Unpaired t test $p = 0.062$, df = 26) and H7N7 (Unpaired t test $p = 0.79$, df = 30) infected animals showed no preference for the new target quadrant (Fig. 5C). No differences between tested groups were detected 120 days pi (Ctrl: Unpaired t test $p = 0.004$, df = 26, H3N2: Unpaired t test $p < 0.0001$, df = 26, H7N7: Unpaired t test $p = 0.048$, df = 30, Fig. 5D).

IAV infection leads to long-term alterations in the function and morphology of hippocampal neurons

Given the observed impairment in cognitive function following H3N2 and H7N7 influenza infection, we were interested whether hippocampal network function would be compromised on a long-term timescale by the IAV infection. For this purpose, we analyzed synaptic plasticity at the Schaffer collateral pathway connecting the CA3 with the CA1 subfield, one of the most extensively studied synapses in the central nervous system (Fig. 6). First, the dependence of the field excitatory postsynaptic potential (fEPSP) slope on stimulation intensity was assessed from input/output curves. Similar input/output relations of CA1 neurons in hippocampal slices from control and influenza A virus infected mice were found for both time points following infection (Two-way ANOVA: F_{30dpi} (2, 27) = 2.53, p = 0.09 and F_{120dpi} (2, 27) = 0.40, p = 0.66 (both factors fixed, number of brain slices in each group = 10), Fig. 6A). In addition, the potential effects of IAV infection on short-term synaptic potentiation of CA1 neurons were investigated 30 and 120 days pi (Fig. 6B). IAV infection did not alter paired-pulse facilitation (PPF) as fEPSP2/fEPSP1 in hippocampal slices at 30 days and 120 days pi were not significantly different between control and infected animals (Two-way ANOVA: F_{30dpi} (2, 30) = 0.06, p = 0.93 and F_{120dpi} (2, 28) = 1.48, p = 0.24 (both factors fixed, number of brain slices in each group = 9-11), Fig. 6B). These results indicate that basal synaptic transmission at individual synapses as well as short-term synaptic plasticity in the CA1 region were not affected by IAV infection.

In addition, long-term synaptic plasticity was investigated. Long-term potentiation (LTP) at the Schaffer collateral CA3 to CA1 pathway was induced by theta-burst stimulation (TBS) after 20 min of baseline recording (Fig. 6C-F). 30 days pi the induction phase of LTP (T 0-5 min after TBS) was significantly reduced only in hippocampal slices derived from H7N7 infected mice (One-way ANOVA F (2, 42) = 3.92, p = 0.02, number of brain slices in each group = 13-17). However, the stable phase of LTP (T 55-60 min after TBS) was significantly decreased in both slices from H3N2 and H7N7 IAV infected mice thereby revealing a significant impairment in synaptic plasticity compared to control hippocampal slices (One-way ANOVA F (2, 42) = 5.74, p = 0.006, Fig. 6C-D). 120 days pi the induction (One-way ANOVA F (2, 35) = 0.30, p = 0.74, number of brain slices in each group = 11-15) and maintenance phase of LTP in both H3N2 and H7N7 were comparable to control slices (One-way ANOVA F (2, 35) = 0.84, p = 0.43, Fig. 6E-F).

As a next step to investigate the potential cellular basis underlying the reduction in LTP and memory impairment, hippocampal neuronal morphology was analyzed 30,

60 and 120 days pi (Fig. 7). Spines are tiny, dendritic protrusions which carry the majority of excitatory synapses in the hippocampus, and changes in spine density can provide information about alterations in the connectivity of hippocampal subregions. Spines were therefore counted separately on apical dendrites of CA1 and CA3 pyramidal neurons as well as on dentate granule cells being located in the superior and inferior blade of the granule cell layer in the hippocampus (Fig. 7A). A significant reduction in dendritic spine density was found in H3N2 (CA1: Δ 17.08%, CA3: Δ 19.24%) and H7N7 (CA1: Δ 22.13%, CA3: Δ 15.02%) infected mice 30 days pi, whereas H1N1 infection had no significant effect compared to control (CA1: Δ 2.28%, CA3: Δ 3.46%) (One-way ANOVA F_{CA1} (3, 186) = 18.97, $p < 0.0001$ and F_{CA3} (3, 196) = 16.40, $p < 0.0001$, Fig. 7A-C). The extent of the phenotype differed between the hippocampal subregions as both in the superior and inferior dentate gyrus, only infection with H7N7 IAV led to a significant reduction in dendritic spine density (DG-superior: Δ 17.08%, DG-inferior: Δ 21.95%) (One-way ANOVA $F_{DG\text{-}superior}$ (3, 186) = 18.15, $p < 0.0001$ and $F_{DG\text{-}inferior}$ (3, 184) = 33.65, $p < 0.0001$, Fig. 7D-E). Further assessment of H3N2 and H7N7 infected animals showed at day 60 pi a partial recovery of the reduced spine density predominantly for the DG and CA3 subregions and more pronounced for H3N2 infected animals (CA1 - H3N2: Δ 10.59% and H7N7: Δ 15.16%, CA3 - H3N2: Δ 7.12% and H7N7: Δ 15.66%, DG-superior - H7N7: Δ 3.78%, DG-inferior - H7N7: Δ 4.88%, Fig. 7B-E). 120 days pi, spine density in H7N7 and H3N2 infected mice was indistinguishable from control animals in all subregions of the hippocampus ($p < 0.0001$ compared to 30 dpi, Fig. 7B-E).

IAV infection enhances glial cell density and activation status within the hippocampus

As processes of prolonged neuroinflammation following IAV infection might be the underlying cause for the alterations observed in this study, ranging from single synapses to neuronal plasticity and eventually affecting mouse behavior, the effects of influenza A viruses on microglia density and activation status in the hippocampus were analyzed. For this purpose, IBA-1 staining was performed (Fig. 8A-C). IBA-1 positive cells were counted and analyzed separately in the CA1, CA3 region and DG superior and inferior blade of the granule cell layer in the hippocampus. Whereas microglia density was not affected 30 days pi with H1N1 (CA1: Δ 4.55%, CA3: Δ 7.67%), microglia density in the CA3 region (Δ 30.25%) and inferior blade of the

dentate gyrus (Δ 27.40%) was increased after H3N2 infection (Fig. 8B). The neurotropic H7N7 IAV infection induced a robust increase in microglia density for all hippocampal subfields analyzed (CA1: Δ 24.67%, CA3: 32.08%, DG-superior: 49.18%, DG-inferior: 55.96%) (One-way ANOVA F_{CA1} (3, 76) = 5.13, p = 0.002, F_{CA3} (3, 76) = 9.90, p < 0.0001, $F_{DG\text{-}superior}$ (3, 76) = 17.57, p < 0.0001 and $F_{DG\text{-}inferior}$ (3, 76) = 22.16, p < 0.0001, Fig. 8B).

In order to determine the activation status of microglia cells in infected individuals compared to control animals, the number of primary processes per cell was quantified (Fig. 8C). For both H3N2 and H7N7 virus types, the number of primary processes per cell decreased in all subregions of the hippocampus 30 days pi (One-way ANOVA F_{CA1} (3, 636) = 178.90, p < 0.0001, F_{CA3} (3, 701) = 259.00, p < 0.0001, $F_{DG\text{-}superior}$ (3, 706) = 155.5, p < 0.0001 and $F_{DG\text{-}inferior}$ (3, 641) = 203.20, p < 0.0001, Fig. 8C) indicating increased activation levels. The strongest reduction was found in the superior and inferior blade of the dentate gyrus upon H7N7 infection (p < 0.001 compared to control and H3N2 IAV infected mice). A partial recovery of microglia density (CA3 - H3N2: Δ 4.80% and H7N7: Δ 12.32%, DG-superior - H7N7: Δ 18.14%, DG-inferior – H3N2: Δ 10.30% and H7N7: Δ 24.27%, Fig. 8B), as well as activation status, occurred in the DG and CA3 subregions 60 days pi, especially in H3N2 infected animals (Fig. 8C). At day 120 pi microglia cell density and activation status in infected mice were comparable to control levels (p < 0.001 compared to 30 dpi, Fig. 8B-C).

In addition to the effect of IAV infection on microglia, we investigated the density of astrocytes in hippocampal subregions using GFAP staining (Fig. 8D-E). Astrocyte density in all subregions of the hippocampus was increased 30 days after infection with H7N7 (CA1: Δ 44.87%, CA3: Δ 45.78%, DG-superior: Δ 14.90%, DG-inferior: Δ 22.60%), whereas only the CA1 (Δ 29.47%) and CA3 (Δ 29.29%) subregion were affected in H3N2 infected animals (Fig. 8E). As was the case for spine density and microglia, H1N1 did not affect astrocyte number in the hippocampus (CA1: Δ 2.73%, CA3: Δ -7.42%) (One-way ANOVA F_{CA1} (3, 36) = 16.07, p < 0.0001, F_{CA3} (3, 36) = 14.10, p < 0.0001, $F_{DG\text{-}superior}$ (3, 35) = 3.31, p = 0.03 and $F_{DG\text{-}inferior}$ (3, 36) = 3.31, p = 0.03, Fig. 8E). As was the case for microglia also on the level of astrocytes a partial and a full recovery comparable to control numbers could be found 60 (H7N7 - CA1: Δ 8.19%, CA3: Δ -7.45%, DG-superior: Δ -7.42%, DG-inferior: Δ -1.80%) and 120 days pi, respectively (p < 0.05 compared to 30 dpi, Fig. 8E).

IAV infection increases blood-brain barrier permeability and cytokine level

As a next step, we examined the integrity of the blood-brain barrier (BBB) following H3N2 and H7N7 IAV infection (Fig. 9). For this purpose, animals were injected with 2% (w/v) Evans blue intraperitoneally at day 4, 8 and 10 post infection. The results of spectrophotometry showed that upon infection with H3N2 and H7N7 IAV an increased Evans blue absorbance and therefore a compromised BBB could be detected on day 8 post infection with H3N2 and H7N7 (One-way ANOVA $F(2, 19) = 8.67$, $p = 0.002$, Fig. 9A). On day 10 post infection, only H7N7 infected mice showed an Evans blue staining well visible already macroscopically in the brain, whereas in the CNS of H3N2 infected mice it was only weakly visible around the ventricles (Fig. 9B).

We were furthermore interested whether cytokines level would be increased as well in the periphery and especially also in the CNS. Therefore, TNF-α and IFN-γ levels were assessed in the periphery and the CNS via ELISA at 8 days post infection (Fig. 9C-H). An earlier study suggested that IFNs and TNF-α have a significant role in priming immune cells for higher cytokine and chemokine production during influenza A virus infection (Veckman et al., 2006). Cytokine levels was quantified in blood serum, CNS in general and in the hippocampus of IAV infected mice. Our data revealed that the levels of IFN-γ and TNF-α were significantly elevated in the blood serum, CNS and hippocampus of H7N7 IAV infected mice (Fig. 9C-H). Interestingly, also infection with the two non-neurotropic influenza virus subtypes led to significantly increased levels of TNF-α in the hippocampus of infected mice compared to control (Fig. 9H) (IFN-γ: one way ANOVA $F_{serum}(3, 10) = 22.37$, $p < 0.0001$, $F_{Brain}(3, 24) = 14.96$, $p < 0.0001$, $F_{Hippocampus}(3, 23) = 9.76$, $p = 0.0002$ and TNF-α: one way ANOVA $F_{serum}(3, 10) = 5.49$, $p = 0.017$, $F_{Brain}(3, 26) = 5.07$, $p = 0.006$, $F_{Hippocampus}(3, 22) = 9.67$, $p = 0.0003$).

IAV infection differentially affects gene expression in the hippocampus

We performed whole genome expression analysis at 18 and 30 days pi to study changes in gene expression in the hippocampus after IAV infection. Since we did not detect long-term alterations in brain morphology, function or cognitive behavior following H1N1 infection, we performed these studies only in H3N2 and H7N7 infected mice. Furthermore, we focused our analysis on the hippocampus where we described functional and morphological alterations (see above). Mock-infected mice

(PBS), sacrificed at the same days post treatment were used as controls. We identified 487 differentially expressed probesets (DEPs) in the hippocampus of animals at day 18 pi with H3N2 virus compared to mock-treated animals. However, no DEPs were found at 30 days post H3N2 infection. After infection with H7N7, 174 DEPs were observed at 18 days pi and also 250 DEPs at 30 days pi compared to mock controls (Fig. 10A). Most of the H3N2-induced differentially expressed genes (DEGs, 342) did not overlap with H7N7-induced DEGs, indicating a virus-specific response in the hippocampus (Fig. 10B).

KEGG (Kyoto Encyclopedia of Genes and Genomes) pathway analysis of DEGs revealed a significant induction of immune responses and inflammatory processes at 18 days after H7N7 IAV infection which continued until day 30 post infection, and at 18 days after H3N2 IAV (Fig. 10C). Especially, genes involved in antigen processing and presentation were found amongst the most strongly upregulated genes following H3N2 and H7N7 IAV infection indicating activation of an immune response in the CNS. Furthermore, KEGG analysis of DEGs in both H3N2 and H7N7 IAV infected mice compared to mock-infected controls (Fig. 10C) revealed DEGs belonging to cell adhesion molecule (CAM) pathways which play a critical role in a wide array of biological processes that include hemostasis, the immune response, inflammation and development of neuronal tissue (Joseph-Silverstein and Silverstein, 1998). Moreover, cell-cell adhesions are important for synaptic function (Bailey et al., 2015).

Our analysis also revealed a significant adverse regulation of microglia-related genes following IAV infection. For instance, an increased expression of microglia signature genes such as *Olfml3* (H3N2: t = 3.60, p = 0.04 and H7N7: t = 5.42, p = 0.03) and *Tmem119* (H3N2: t = 2.49, p = 0.1 and H7N7: t = 3.44, p = 0.09) and downregulation of the microglia-neuron crosstalk gene (*Cx3cr1*) (H3N2: t = -4.39, p = 0.02 and H7N7: t = -2.04, p = 0.1) were observed following both H3N2 and H7N7 IAV infection (Fig. 10D). Furthermore, the analysis of genes reflecting microglia activation and in particular the MHC class II family (antigen processing and presentation), microglial-mediated phagocytosis (*Fcgr4*, *Dap12* and *Ctsz*) (*Fcgr4*: t = 4.68, p = 0.05, *Dap12*: 4.54, p = 0.05 and *Ctsz*: t = 4.73, p = 0.04) and complement system genes (*C1qa*, *C1qb*, *C1qc* and *Vwf*) (*C1qa*: t = 6.31, p = 0.03, *C1qb*: 5.16, p = 0.04, *C1qc*: t = 3.28, p = 0.1 and *Vwf*: t = 4.27, p = 0.06) revealed a significant upregulation especially in the group of H7N7 infected animals (Fig. 10D). In addition to microglia, an increased expression of astrocyte signature and activation genes such as *Gfap* (H3N2: t = 2.94,

p = 0.08 and H7N7: t = 3.16, p = 0.1) and *Psmb8* (H3N2: t = 3.65, p = 0.04 and H7N7: t = 4.44, p = 0.05) (Table 1) was observed in the hippocampus of H3N2 and H7N7 IAV infected mice.

Rbfox3 (NeuN) (H3N2: t = -4.07, p = 0.03 and H7N7: t = -3.94, p = 0.07), *Nrcam* (neuronal cell adhesion molecule) (H3N2: t = -5.99, p = 0.01 and H7N7: t = -4.98, p = 0.04) and *Cacna1c* (voltage-dependent calcium channel) (H3N2: t = -3.75, p = 0.04 and H7N7: t = -6.61, p = 0.03) were diminished similarly in H3N2 and H7N7 IAV infected groups 18 days pi (Table 1). Dysfunction of these genes has been identified in several neurodevelopmental and neuropsychiatric disorders such as autism, schizophrenia and cognitive impairments (Demyanenko et al., 2014; Lee et al., 2016; Lin et al., 2016). In addition, *Rbfox3* knockout mice show deficits in synaptic transmission and plasticity in the dentate gyrus (Wang et al., 2015). Moreover, down-regulation of the neurotrophic factors *Bdnf* (H3N2: t = -3.52, p = 0.05 and H7N7: t = -3.66, p = 0.08) and *Ntf3* (H3N2: t = -6.88, p = 0.009 and H7N7: t = -3.91, p = 0.07) as well as a number of important solute carriers such as *Slc4a7* (bicarbonate cotransporter, H3N2: t = -4.87, p = 0.02 and H7N7: t = -5.03, p = 0.04), *Slc30a5* (zinc transporter, H3N2: t = -4.78, p = 0.02 and H7N7: t = -3.56, p = 0.09), S*lc2a1* (glucose transporter, GLUT-1, H3N2: t = -3.27, p = 0.06 and H7N7: t = -3.69, p = 0.08) and *Slc1a2* (glutamate transporter, H3N2: t = -4.70, p = 0.02 and H7N7: t = -3.43, p = 0.05), and synapse-associated protein genes including *Grm5* (glutamate receptor, H3N2: t = -3.87, p = 0.03 and H7N7: t = -2.49, p = 0.1) and *Dlg3* (SAP102, H3N2: t = -4.79, p = 0.02 and H7N7: t = -3.67, p = 0.08) were observed irrespective of the virus subtype (Table 1). It is known that SAP102 null mice exhibit impaired spatial learning along with defects in synaptic plasticity (Cuthbert, 2007). It is also worth noting that following both H3N2 and H7N7 IAV infection, upregulation of interferon-response related genes including *Psmb9* (H3N2: t = 3.04, p = 0.08 and H7N7: t = 4.62, p = 0.05), *Lgals3bp* (H3N2: t = 3.67, p = 0.04 and H7N7: t = 4.51, p = 0.05), *Oas2* (H3N2: t = 6.24, p = 0.01 and H7N7: t = 5.28, p = 0.04) and especially *Ccl5* (H3N2: t = 4.46, p = 0.02 and H7N7: t = 3.93, p = 0.07) were observed, the latter one has been previously associated with cognitive decline (Laurent et al., 2017) (Table 1).

Discussion

Influenza is primarily considered as a respiratory disease. However, evidence accumulates that an infection with influenza A viruses (IAV) may also be associated

with neurological complications in humans (Surana et al., 2011; Ekstrand, 2012; Shah et al., 2014). As influenza viruses can be either neurotropic or non-neurotropic it is important to discriminate between alterations directly mediated by the fact that the virus is actually able to replicate in the brain and, on the other hand, CNS complications as a result of the host immune response in the periphery. Here, we investigated the long-term neurological impact of an infection with either neurotropic or non-neurotropic IAV subtypes. The long-lasting consequences of an influenza infection on the brain have not been studied before. Our findings provide evidence that neuroinflammation caused by non-neurotropic and neurotropic influenza viruses induces long-lasting impairments in hippocampal neuronal morphology and synaptic properties as well as cognitive function in adult animals.

A comparison of the two non-neurotropic viruses H1N1 and H3N2 revealed that infection with H1N1 did not lead to any long-term alterations in spatial memory formation and neuron morphology. In a previous study, H1N1 infected mice showed impairment in the reversal task in the Morris water maze suggesting influenza-induced cognitive deficits during the acute phase of the infection (Jurgens et al., 2012). While our results showed that recovery from the infection with this variant seems to be fast, the infection with the non-neurotropic H3N2 subtype and neurotropic H7N7 caused long-lasting cognitive deficits in infected animals. We therefore concentrated on a detailed comparison between infection with H3N2 which is not able to replicate in the brain and H7N7 where we indeed could detect replicating virus in the CNS.

Infection with both virus subtypes led to a compromised BBB 8 days post infection. This is in line with an elevation of cytokine levels in the CNS detected here. Although the concentration of IFN-γ and TNF-α was highest in the case of H7N7 infection both in the serum and in the CNS also infection with H3N2 led to significantly elevated levels of TNF-α in the hippocampus. Indeed, several studies indicate that after different types of infection in the periphery or the brain an increased inflammatory gene expression, e.g. IL-1ß, IL-6, TNF-α and IFN-γ, can be observed across multiple brain regions, including the hippocampus (Howe et al., 2012; Elmore et al., 2014; Heneka et al., 2014; Klein et al., 2017). The cytokines generated during peripheral inflammation can activate a secondary, mirror inflammatory response (indirect, immune response-mediated pathways) in the brain that is characterized by activation of microglia and production of pro-inflammatory cytokines, most importantly, TNF-α,

IL-1 and IL-6 (Riazi et al., 2015). Indeed, we were able to detect an increase in the number of microglia in the hippocampus of H3N2 and H7N7 infected mice which could at least in parts be attributable to the leaky BBB following influenza infection. Although activated microglia are crucial for the host defense against pathogens, prolonged or aberrant activation can have damaging effects on neurons and can adversely affect synaptic transmission and structure (Hanisch, 2002; Block et al., 2007; Pickering and O'Connor, 2007; Riazi et al., 2015). It was shown previously that microglia can also play a role in synaptic remodeling and plasticity in the healthy brain (Nimmerjahn et al., 2005; Parkhurst et al., 2013) for instance via neuron-microglia crosstalk through the *Cx3cr1* signaling axis which we found to be downregulated independently of the virus subtype. The observed long-term alterations in spine number, synaptic plasticity and cognitive function following IAV infection might therefore indeed result in parts from a general virus subtype-independent hyperactivation of microglia cells in the hippocampus triggered through the immune response to the influenza virus in the periphery. In this respect, it was shown previously that pro-inflammatory mediators produced during the infection affected neuronal morphology, synaptic structure and function (Yirmiya and Goshen, 2011; Estes and McAllister, 2015). In particular, chronic inflammation *in vivo* and exposure of cultured brain cells to lipopolysaccharide (LPS) *in vitro* led to a loss of spines reminiscent to changes found in many neurological diseases (Chang et al., 2015). Furthermore, manipulation of individual cytokines can modulate learning, memory formation, and synaptic plasticity (Marin and Kipnis, 2013; Donzis and Tronson, 2014). The increased production of inflammatory mediators from brain immune cells might indeed disrupt the delicate balance in the neuro-microglia crosstalk (Tanaka et al., 2006; Yirmiya and Goshen, 2011).

The number of astrocytes was increased as well following infection with neurotropic and non-neurotropic IAV subtypes. We detected a downregulation of astrocyte specific glutamate transporter *Slc1a2* levels which plays an essential role in the maintenance of normal excitatory synaptic transmission, protection of neurons from the excitotoxicity of excessive glutamate, and regulation of glutamate-mediated neuroplasticity (David et al., 2009). Interestingly, in both H3N2 and H7N7 infected mice elevated numbers of astrocytes recovered faster than the number and activation status of microglia cells suggesting that an astrocyte-microglial interaction might be a key mechanism for the regulation of brain inflammation during influenza

infection. In this regard, previous findings suggest that astrocytes can regulate microglial activity by stimulating their antioxidant gene expression, perhaps providing a negative feedback response to titrate the inflammatory reaction induced by pro-inflammatory mechanisms thus modulating microglial resting status versus activation state (Shih et al., 2006).

Besides the striking similarity of the phenotypes on the general level of glial cell and synapse number as well as the gene expression profiles following infection with non-neurotropic and neurotropic IAV subtypes pointing towards immune response-mediated indirect pathways we were able to reveal also characteristic differences in the long-lasting outcome following infection with these two viruses. Infection with the neurotropic virus led to synapse loss in all three hippocampal subregions together with a robust impairment in spatial map formation whereas H3N2 infection was associated with synapse loss only in the *cornu ammonis* region and a reduced ability to update the new platform position in the reversal phase but almost normal learning in the initial water maze task. It was indeed shown previously that the progressive nature of neurotropic virus-induced damage in the dentate gyrus such for instance during Borna virus infection is associated with impaired performance in the Morris water maze (Rubin et al., 1999). Moreover, there is evidence that the plain water maze task can efficiently be solved despite LTP impairments in either the CA1 or the CA3 region (Nakazawa et al., 2002; Bannerman et al., 2012). Our data therefore show that hippocampal subregions might indeed exhibit a different sensitivity to inflammation induced damage with the DG being more resilient. Moreover, our results indicate that the neuronal representation of behavioral flexibility to decide between competing memories in the reversal task may reside more in the CA1 and CA3 subfield than in the DG.

In case of the neurotropic virus H7N7 we observed a much stronger reaction which was consistent throughout all hippocampal subregions including the dentate gyrus. In this respect it is interesting to note that the interferon-responsive gene *Ifit3* which is reported to be involved in cognitive decline in aged mice (Bordner et al., 2011) was specifically upregulated in the hippocampus of H7N7 IAV infected mice, and is mainly expressed in granule cells (Cho et al., 2013). This indicates that the direct presence of the virus in the brain leads to even more detrimental effects (direct, virus-mediated pathways). The gene expression profile analysis revealed that the increase in microglia activation markers was even stronger in H7N7 infected individuals

877 compared to H3N2 infected mice. Especially the levels of genes belonging to the
878 major histocompatibility class 2 family (MHCII) were strongly increased indicating
879 direct contact of microglia and the IAV.
880 Evidence now accumulates that chronic neuroinflammation may be a central
881 mechanism contributing to the generation and progression of a number of
882 neuropsychiatric and neurodegenerative disorders including Alzheimer´s disease
883 (Frank-Cannon et al., 2009; Heneka et al., 2014). Interestingly, the dopamine
884 neurotransmitter transporter gene *Slc6a3* which has been associated with depression
885 and other neuropsychiatric disorders (Sinanan and Hillary, 1981; Uddin et al., 2011)
886 was among the most strongly upregulated genes especially after H7N7 infection.
887 Thus, our findings have significant implications for the clinical consequences of IAV
888 infections. An influenza infection with neurotropic viruses but also infections with a
889 non-neurotropic virus can initiate inflammatory cascades via microglia and astrocyte
890 activation in the brain and therefore increase the likelihood to develop
891 neuropsychiatric and neurodegenerative disorders. The host immune response
892 triggered by a lung infection with H3N2 was able to impair hippocampal function. But
893 more so, replication of an influenza virus in the brain resulted in a stronger and more
894 prolonged activation of microglia with detrimental outcome for cognitive functions. In
895 our study, we only worked with younger animals. It will thus be important to study if
896 similar or even more pronounced impairments were observed in aged mice and if the
897 developing brains in newborn and juvenile individuals could also be affected.
898 Approaches to regulate glial cell activity may provide a future strategy to prevent
899 deleterious long-term effects on the brain, especially in highly vulnerable patient
900 groups.

References

Bailey CH, Kandel ER, Harris KM (2015) Structural components of synaptic plasticity and memory consolidation. Cold Spring Harbor Perspectives in Biology 7:a021758.

Banks J, Speidel E, Alexander DJ (1998) Characterisation of an avian influenza A virus isolated from a human--is an intermediate host necessary for the emergence of pandemic influenza viruses? Archives of virology 143:781-787.

Bannerman DM, Bus T, Taylor A, Sanderson DJ, Schwarz I, Jensen V, Hvalby O, Rawlins JN, Seeburg PH, Sprengel R (2012) Dissecting spatial knowledge from spatial choice by hippocampal NMDA receptor deletion. Nature neuroscience 15:1153-1159.

Bao Y, Gao Y, Shi Y, Cui X (2017) Dynamic gene expression analysis in a H1N1 influenza virus mouse pneumonia model. Virus genes 53:357-366.

Benjamini Y, Hochberg Y (1995) Controlling the false discovery rate: A practical and powerful apporach to multiple testing. Journal of the Royal Statistical Society 57:289-300.

Blazejewska P, Koscinski L, Viegas N, Anhlan D, Ludwig S, Schughart K (2011) Pathogenicity of different PR8 influenza A virus variants in mice is determined by both viral and host factors. Virology 412:36-45.

Block ML, Zecca L, Hong JS (2007) Microglia-mediated neurotoxicity: uncovering the molecular mechanisms. Nature reviews Neuroscience 8:57-69.

Bordner KA, Kitchen RR, Carlyle B, George ED, Mahajan MC, Mane SM, Taylor JR, Simen AA (2011) Parallel declines in cognition, motivation, and locomotion in aging mice: association with immune gene upregulation in the medial prefrontal cortex. Experimental gerontology 46:643-659.

Brahmachari S, Fung YK, Pahan K (2006) Induction of glial fibrillary acidic protein expression in astrocytes by nitric oxide. The Journal of neuroscience : the official journal of the Society for Neuroscience 26:4930-4939.

Camara ML, Corrigan F, Jaehne EJ, Jawahar MC, Anscomb H, Baune BT (2015) Effects of centrally administered etanercept on behavior, microglia, and astrocytes in mice following a peripheral immune challenge. Neuropsychopharmacology : official publication of the American College of Neuropsychopharmacology 40:502-512.

Carlson M (2014) MmAgilentDesign026655.db: Agilent Chips that use Agilent design number 026655 annotation data (chip MmAgilentDesign026655).R package version 2.14.0. http://www.bioconductor.org/packages/release/data/annotation/html/MmAgilentDesign026655.db.html.

CDC (2012) Severe influenza among children and young adults with neurologic and neurodevelopmental conditions - Ohio, 2011. MMWR Morbidity and mortality weekly report 60:1729-1733.

Chang PK, Khatchadourian A, McKinney RA, Maysinger D (2015) Docosahexaenoic acid (DHA): a modulator of microglia activity and dendritic spine morphology. Journal of neuroinflammation 12:34.

Cho H, Proll SC, Szretter KJ, Katze MG, Gale Jr M, Diamond MS (2013) Differential innate immune response programs in neuronal subtypes determine susceptibility to infection in the brain by positive-stranded RNA viruses. Nature medicine 19:458-464.

Cooper DS, Saxena NC, Yang HS, Lee HJ, Moring AG, Lee A, Choi I (2005) Molecular and functional characterization of the electroneutral Na/HCO3 cotransporter NBCn1 in rat hippocampal neurons. The Journal of biological chemistry 280:17823-17830.

946 Crotti A, Ransohoff RM (2016) Microglial physiology and pathophysiology: insights from
947 genome-wide transcriptional profiling. Immunity 44:505-515.

948 Cuthbert PC (2007) Synapse-Associated Protein 102/dlgh3 Couples the NMDA Receptor to
949 Specific Plasticity Pathways and Learning Strategies. 27:2673-2682.

950 D'Hooge R, De Deyn PP (2001) Applications of the Morris water maze in the study of
951 learning and memory. Brain research Brain research reviews 36:60-90.

952 David Y, Cacheaux LP, Ivens S, Lapilover E, Heinemann U, Kaufer D, Friedman A (2009)
953 Astrocytic dysfunction in epileptogenesis: consequence of altered potassium and
954 glutamate homeostasis? Journal of Neuroscience 29:10588-10599.

955 Demyanenko GP, Mohan V, Zhang X, Brennaman LH, Dharbal KES, Tran TS, Manis PB,
956 Maness PF (2014) Neural Cell Adhesion Molecule NrCAM Regulates Semaphorin
957 3F-Induced Dendritic Spine Remodeling. The Journal of neuroscience : the official
958 journal of the Society for Neuroscience 34:11274-11287.

959 Donzis EJ, Tronson NC (2014) Modulation of learning and memory by cytokines: signaling
960 mechanisms and long term consequences. Neurobiology of learning and memory
961 115:68-77.

962 Ekstrand JJ (2012) Neurologic complications of influenza. Seminars in pediatric neurology
963 19:96-100.

964 Elmore MR, Burton MD, Conrad MS, Rytych JL, Van Alstine WG, Johnson RW (2014)
965 Respiratory viral infection in neonatal piglets causes marked microglia activation in
966 the hippocampus and deficits in spatial learning. The Journal of neuroscience : the
967 official journal of the Society for Neuroscience 34:2120-2129.

968 Estes ML, McAllister AK (2015) Immune mediators in the brain and peripheral tissues in
969 autism spectrum disorder. Nature reviews Neuroscience 16:469-486.

970 Fouchier RA, Schneeberger PM, Rozendaal FW, Broekman JM, Kemink SA, Munster V,
971 Kuiken T, Rimmelzwaan GF, Schutten M, Van Doornum GJ, Koch G, Bosman A,
972 Koopmans M, Osterhaus AD (2004) Avian influenza A virus (H7N7) associated with
973 human conjunctivitis and a fatal case of acute respiratory distress syndrome.
974 Proceedings of the National Academy of Sciences of the United States of America
975 101:1356-1361.

976 Frank-Cannon TC, Alto LT, McAlpine FE, Tansey MG (2009) Does neuroinflammation fan
977 the flame in neurodegenerative diseases? Molecular neurodegeneration 4:47.

978 Gabriel G, Dauber B, Wolff T, Planz O, Klenk HD, Stech J (2005) The viral polymerase
979 mediates adaptation of an avian influenza virus to a mammalian host. Proceedings of
980 the National Academy of Sciences of the United States of America 102:18590-18595.

981 Garthe A, Kempermann G (2013) An old test for new neurons: refining the Morris water
982 maze to study the functional relevance of adult hippocampal neurogenesis. Frontiers
983 in neuroscience 7:63.

984 Garthe A, Behr J, Kempermann G (2009) Adult-generated hippocampal neurons allow the
985 flexible use of spatially precise learning strategies. PloS one 4:e5464.

986 Gentleman RC et al. (2004) Bioconductor: open software development for computational
987 biology and bioinformatics. Genome biology 5:R80.

988 Gerhauser I, Alldinger S, Baumgärtner W (2007) Ets-1 represents a pivotal transcription
989 factor for viral clearance, inflammation, and demyelination in a mouse model of
990 multiple sclerosis. Journal of neuroimmunology 188:86-94.

991 Geurs TL, Hill EB, Lippold DM, French AR (2012) Sex differences in murine susceptibility to
992 systemic viral infections. Journal of autoimmunity 38:J245-J253.

993 Goffinet C (2016) Cellular Antiviral Factors that Target Particle Infectivity of HIV-1. Current
994 HIV Research 14:211-216.

995 Haller O, Arnheiter H, Lindenmann J (1979) Natural, genetically determined resistance
996 toward influenza virus in hemopoietic mouse chimeras. Role of mononuclear
997 phagocytes. The Journal of experimental medicine 150:117-126.

998 Hanisch UK (2002) Microglia as a source and target of cytokines. Glia 40:140-155.

999 Heneka MT, Kummer MP, Latz E (2014) Innate immune activation in neurodegenerative
1000 disease. Nature reviews Immunology 14:463-477.

1001 Hodgson NR, Bohnet SG, Majde JA, Krueger JM (2012) Influenza virus pathophysiology and
1002 brain invasion in mice with functional and dysfunctional Mx1 genes. Brain, behavior,
1003 and immunity 26:83-89.

1004 Hogg S (1996) A review of the validity and variability of the elevated plus-maze as an animal
1005 model of anxiety. Pharmacology, biochemistry, and behavior 54:21-30.

1006 Howe CL, Lafrance-Corey RG, Sundsbak RS, Lafrance SJ (2012) Inflammatory monocytes
1007 damage the hippocampus during acute picornavirus infection of the brain. Journal of
1008 neuroinflammation 9:50.

1009 Hoyo-Becerra C, Liu Z, Yao J, Kaltwasser B, Gerken G, Hermann DM, Schlaak JF (2015)
1010 Rapid Regulation of Depression-Associated Genes in a New Mouse Model Mimicking
1011 Interferon-alpha-Related Depression in Hepatitis C Virus Infection. Molecular
1012 Neurobiology 52:318-329.

1013 Hristovska I, Pascual O (2015) Deciphering Resting Microglial Morphology and Process
1014 Motility from a Synaptic Prospect. Frontiers in Integrative Neuroscience 9.

1015 Huang EJ, Reichardt LF (2001) Neurotrophins: Roles in Neuronal Development and
1016 Function. Annual review of neuroscience 24:677-736.

1017 Jang H, Boltz D, Sturm-Ramirez K, Shepherd KR, Jiao Y, Webster R, Smeyne RJ (2009)
1018 Highly pathogenic H5N1 influenza virus can enter the central nervous system and
1019 induce neuroinflammation and neurodegeneration. Proceedings of the National
1020 Academy of Sciences of the United States of America 106:14063-14068.

1021 Jang H, Boltz D, McClaren J, Pani AK, Smeyne M, Korff A, Webster R, Smeyne RJ (2012)
1022 Inflammatory effects of highly pathogenic H5N1 influenza virus infection in the CNS of
1023 mice. The Journal of neuroscience : the official journal of the Society for
1024 Neuroscience 32:1545-1559.

1025 Joseph-Silverstein J, Silverstein RL (1998) Cell adhesion molecules: an overview. Cancer
1026 investigation 16:176-182.

1027 Jurgens HA, Amancherla K, Johnson RW (2012) Influenza infection induces
1028 neuroinflammation, alters hippocampal neuron morphology, and impairs cognition in
1029 adult mice. The Journal of neuroscience : the official journal of the Society for
1030 Neuroscience 32:3958-3968.

1031 Klein RS, Garber C, Howard N (2017) Infectious immunity in the central nervous system and
1032 brain function. Nat Immunol 18:132-141.

1033 Korte M, Schmitz D (2016) Cellular and System Biology of Memory: Timing, Molecules, and
1034 Beyond. Physiological reviews 96:647-693.

1035 Kristensson K (2006) Avian influenza and the brain--comments on the occasion of
1036 resurrection of the Spanish flu virus. Brain research bulletin 68:406-413.

1037 Lang G, Gagnon A, Geraci JR (1981) Isolation of an influenza A virus from seals. Archives of
1038 virology 68:189-195.

1039 Laurent C et al. (2017) Hippocampal T cell infiltration promotes neuroinflammation and
1040 cognitive decline in a mouse model of tauopathy. Brain 140:184-200.

1041 Lee AS, De Jesus-Cortes H, Kabir ZD, Knobbe W, Orr M, Burgdorf C, Huntington P,
1042 McDaniel L, Britt JK, Hoffmann F, Brat DJ, Rajadhyaksha AM, Pieper AA (2016) The
1043 Neuropsychiatric Disease-Associated Gene cacna1c Mediates Survival of Young
1044 Hippocampal Neurons. eNeuro 3.

1045 Leist SR, Pilzner C, van den Brand JM, Dengler L, Geffers R, Kuiken T, Balling R, Kollmus
1046 H, Schughart K (2016) Influenza H3N2 infection of the collaborative cross founder
1047 strains reveals highly divergent host responses and identifies a unique phenotype in
1048 CAST/EiJ mice. BMC genomics 17:143.

1049 Lin YS, Wang HY, Huang DF, Hsieh PF, Lin MY, Chou CH, Wu IJ, Huang GJ, Gau SS,
1050 Huang HS (2016) Neuronal Splicing Regulator RBFOX3 (NeuN) Regulates Adult
1051 Hippocampal Neurogenesis and Synaptogenesis. PloS one 11:e0164164.

1052 Liu Y, Liu F, Iqbal K, Grundke-Iqbal I, Gong CX (2008) Decreased glucose transporters
1053 correlate to abnormal hyperphosphorylation of tau in Alzheimer disease. FEBS letters
1054 582:359-364.

1055 Lovell M (2009) A Potential Role for Alterations of Zinc and Zinc Transport Proteins in the
1056 Progression of Alzheimer's Disease. Journal of Alzheimer's disease : JAD 16:471-
1057 483.

1058 Lynch MA (2002) Interleukin-1 beta exerts a myriad of effects in the brain and in particular in
1059 the hippocampus: analysis of some of these actions. Vitamins and hormones 64:185-
1060 219.

1061 Majde JA, Bohnet SG, Ellis GA, Churchill L, Leyva-Grado V, Wu M, Szentirmai E, Rehman
1062 A, Krueger JM (2007) Detection of mouse-adapted human influenza virus in the
1063 olfactory bulbs of mice within hours after intranasal infection. Journal of neurovirology
1064 13:399-409.

1065 Majumdar D, Bevensee MO (2010) Na-coupled bicarbonate transporters of the Slc4 family in
1066 the nervous system: function, localization, and relevance to neurologic function.
1067 Neuroscience 171:951-972.

1068 Manaenko A, Chen H, Kammer J, Zhang JH, Tang J (2011) Comparison Evans Blue
1069 injection routes: intravenous versus intraperitoneal, for measurement of blood–brain
1070 barrier in a mice hemorrhage model. Journal of neuroscience methods 195:206-210.

1071 Marin I, Kipnis J (2013) Learning and memory… and the immune system. Learning &
1072 Memory 20:601-606.

1073 Morawietz G, Ruehl-Fehlert C, Kittel B, Bube A, Keane K, Halm S, Heuser A, Hellmann J
1074 (2004) Revised guides for organ sampling and trimming in rats and mice--Part 3. A
1075 joint publication of the RITA and NACAD groups. Experimental and toxicologic
1076 pathology : official journal of the Gesellschaft fur Toxikologische Pathologie 55:433-
1077 449.

1078 Morris R (1984) Developments of a water-maze procedure for studying spatial learning in the
1079 rat. Journal of neuroscience methods 11:47-60.

1080 Nakazawa K, Quirk MC, Chitwood RA, Watanabe M, Yeckel MF, Sun LD, Kato A, Carr CA,
1081 Johnston D, Wilson MA, Tonegawa S (2002) Requirement for hippocampal CA3
1082 NMDA receptors in associative memory recall. Science (New York, NY) 297:211-218.

1083 Nimmerjahn A, Kirchhoff F, Helmchen F (2005) Resting microglial cells are highly dynamic
1084 surveillants of brain parenchyma in vivo. Science (New York, NY) 308:1314-1318.

1085 Nuttall JR, Oteiza PI (2014) Zinc and the aging brain. Genes & Nutrition 9.

1086 Orre M, Kamphuis W, Dooves S, Kooijman L, Chan ET, Kirk CJ, Dimayuga Smith V, Koot S,
1087 Mamber C, Jansen AH, Ovaa H, Hol EM (2013) Reactive glia show increased
1088 immunoproteasome activity in Alzheimer's disease. Brain 136:1415-1431.

1089 Parkhurst CN, Yang G, Ninan I, Savas JN, Yates JR, Lafaille JJ, Hempstead BL, Littman DR,
1090 Gan WB (2013) Microglia promote learning-dependent synapse formation through
1091 BDNF. Cell 155:1596-1609.

1092 Pickering M, O'Connor JJ (2007) Pro-inflammatory cytokines and their effects in the dentate
1093 gyrus. Progress in brain research 163:339-354.

1094 R_Core_Team (2013a) R: A Language and Environment for Statistical Computing. R
1095 Foundation for Statistical Computing, Vienna, Austria , http://www.R-project.org/. In.

1096 Raison CL, Capuron L, Miller AH (2006) Cytokines sing the blues: inflammation and the
1097 pathogenesis of depression. Trends in immunology 27:24-31.

1098 Riazi K, Galic MA, Kentner AC, Reid AY, Sharkey KA, Pittman QJ (2015) Microglia-
1099 dependent alteration of glutamatergic synaptic transmission and plasticity in the
1100 hippocampus during peripheral inflammation. The Journal of neuroscience : the
1101 official journal of the Society for Neuroscience 35:4942-4952.

1102 Richwine AF, Parkin AO, Buchanan JB, Chen J, Markham JA, Juraska JM, Johnson RW
1103 (2008) Architectural changes to CA1 pyramidal neurons in adult and aged mice after
1104 peripheral immune stimulation. Psychoneuroendocrinology 33:1369-1377.

1105 Rubin SA, Sylves P, Vogel M, Pletnikov M, Moran TH, Schwartz GJ, Carbone KM (1999)
1106 Borna disease virus-induced hippocampal dentate gyrus damage is associated with
1107 spatial learning and memory deficits. Brain research bulletin 48:23-30.

1108 Shah S, Keil A, Gara K, Nagarajan L (2014) Neurologic complications of influenza. Journal of
1109 child neurology 29:Np49-53.

1110 Shih AY, Fernandes HB, Choi FY, Kozoriz MG, Liu Y, Li P, Cowan CM, Klegeris A (2006)
1111 Policing the police: astrocytes modulate microglial activation. The Journal of
1112 neuroscience : the official journal of the Society for Neuroscience 26:3887-3888.

1113 Shinya K, Suto A, Kawakami M, Sakamoto H, Umemura T, Kawaoka Y, Kasai N, Ito T (2005)
1114 Neurovirulence of H7N7 influenza A virus: brain stem encephalitis accompanied with
1115 aspiration pneumonia in mice. Archives of virology 150:1653-1660.

1116 Sinanan K, Hillary I (1981) Post-influenzal depression. The British journal of psychiatry : the
1117 journal of mental science 138:131-133.

1118 Smyth GK (2004) Linear models and empirical bayes methods for assessing differential
1119 expression in microarray experiments. Statistical applications in genetics and
1120 molecular biology 3:Article3.

1121 Surana P, Tang S, McDougall M, Tong CY, Menson E, Lim M (2011) Neurological
1122 complications of pandemic influenza A H1N1 2009 infection: European case series
1123 and review. European journal of pediatrics 170:1007-1015.

1124 Szretter KJ, Balish AL, Katz JM (2006) Influenza: propagation, quantification, and storage.
1125 Current protocols in microbiology Chapter 15:Unit 15G.11.

1126 Tanaka S, Ide M, Shibutani T, Ohtaki H, Numazawa S, Shioda S, Yoshida T (2006)
1127 Lipopolysaccharide-induced microglial activation induces learning and memory
1128 deficits without neuronal cell death in rats. Journal of neuroscience research 83:557-
1129 566.

1130 Thomson CA, McColl A, Cavanagh J, Graham GJ (2014) Peripheral inflammation is
1131 associated with remote global gene expression changes in the brain. Journal of
1132 neuroinflammation 11:73.

1133 Tomonaga K (2004) Virus-induced neurobehavioral disorders: mechanisms and implications.
1134 Trends in molecular medicine 10:71-77.

1135 Tong L, Balazs R, Soiampornkul R, Thangnipon W, Cotman CW (2008) Interleukin-1 beta
1136 impairs brain derived neurotrophic factor-induced signal transduction. Neurobiology of
1137 aging 29:1380-1393.

1138 Tong L, Prieto GA, Kramar EA, Smith ED, Cribbs DH, Lynch G, Cotman CW (2012) Brain-
1139 derived neurotrophic factor-dependent synaptic plasticity is suppressed by
1140 interleukin-1beta via p38 mitogen-activated protein kinase. The Journal of
1141 neuroscience : the official journal of the Society for Neuroscience 32:17714-17724.

1142 Uddin M, Koenen KC, Aiello AE, Wildman DE, de los Santos R, Galea S (2011) Epigenetic
1143 and inflammatory marker profiles associated with depression in a community-based
1144 epidemiologic sample. Psychological Medicine 41:997-1007.

1145 Vasek MJ et al. (2016) A complement-microglial axis drives synapse loss during virus-
1146 induced memory impairment. Nature 534:538-543.

1147 Veckman V, Österlund P, Fagerlund R, Melén K, Matikainen S, Julkunen I (2006) TNF-α and
1148 IFN-α enhance influenza-A-virus-induced chemokine gene expression in human A549
1149 lung epithelial cells. Virology 345:96-104.

1150 Vitkovic L, Konsman JP, Bockaert J, Dantzer R, Homburger V, Jacque C (2000) Cytokine
1151 signals propagate through the brain. Molecular psychiatry 5:604-615.

1152 Vorhees CV, Williams MT (2006) Morris water maze: procedures for assessing spatial and
1153 related forms of learning and memory. Nature protocols 1:848-858.

1154 Walsh RN, Cummins RA (1976) The open-field test: A critical review. Psychological bulletin
1155 83:482.

1156 Wang H-Y, Hsieh P-F, Huang D-F, Chin P-S, Chou C-H, Tung C-C, Chen S-Y, Lee L-J, Gau
1157 SS-F, Huang H-S (2015) RBFOX3/neuN is required for hippocampal circuit balance
1158 and function. Scientific reports 5:17383.

1159 Whishaw IQ (2004) Posterior neocortical (visual cortex) lesions in the rat impair matching-to-
1160 place navigation in a swimming pool: a reevaluation of cortical contributions to spatial
1161 behavior using a new assessment of spatial versus non-spatial behavior. Behavioural
1162 brain research 155:177-184.

1163 Wilk E, Schughart K (2012) The Mouse as Model System to Study Host-Pathogen
1164 Interactions in Influenza A Infections. Current protocols in mouse biology 2:177-205.

1165 Yirmiya R, Goshen I (2011) Immune modulation of learning, memory, neural plasticity and
1166 neurogenesis. Brain, behavior, and immunity 25:181-213.

1167 Yu G, Wang LG, Han Y, He QY (2012) clusterProfiler: an R package for comparing biological
1168 themes among gene clusters. Omics : a journal of integrative biology 16:284-287.

Figure legends

Figure 1. Female C57BL/6J mice were infected intranasally with the indicated viruses and dosages. (A) Body weight loss depicted as percentage of the starting weight of mice during the acute phase of IAV infection is shown (N = 10-18 in each group). (B) Brains of infected mice were tested for the presence of infectious virus in embryonated eggs. Positivity in a hemagglutination assay is displayed as number of positive samples/number of tested samples. Positive samples from the indicated days were titrated by determining EID_{50} (egg infectious dose 50)/ml. (C) Representative sections from the immunohistochemical analysis, hippocampus (left) and medulla oblongata (right) of mice 7 days after intranasal infection with H3N2 (maHK68) (upper row) and H7N7 (rSC35M) (lower row) IAV subtypes. Immunohistochemistry did not reveal influenza nucleoprotein (NP) in the hippocampus and medulla oblongata of H3N2 infected mice and hippocampus of H7N7 infected mice, whereas high numbers of virus infected cells in the medulla oblongata of H7N7 infected mice were detected (Scale bars = 200 µm). Sections were counterstained with Mayer's hematoxylin. Inserts: Higher magnifications of the respective images (Scale bars = 33 µm). (D) In the medulla oblongata of a mouse at 9 days after intranasal H7N7 infection, severe lymphohistiocytic meningitis, few numbers of inflammatory cells in the parenchyma, and a moderate gliosis (center of the image) were observed (Scale bars = 80 µm). Upper insert: Note degenerating cells in higher magnification (arrow). Lower insert: Viral antigen was found in one cell (arrow) using immunohistochemistry for influenza nucleoprotein and Mayer's hematoxylin as counterstaining (Scale bars = 33 µm). (E) H&E staining from brains of H3N2 and H7N7 infected mice were scored semi-quantitatively for signs of inflammation at the respective days (N = 3-5). (F) Immunohistochemistry of viral NP was scored semi-quantitatively (N = 4-5). Data are presented as mean ± SEM.

Figure 2. Long-term effect of influenza A virus infection on general locomotion and willingness to explore in the open field test and anxiety-like behavior in the elevated plus maze test. (A), (B) At 30 and 120 days pi a total distance traveled (One-way ANOVA - 30 dpi (N = 7-10): $F(3, 29) = 2.12$, $p = 0.11$ and 120 dpi (N = 7-8): $F(2, 19) = 6.19$, $p = 0.08$), average speed (One-way ANOVA - 30 dpi (N = 7-10): $F(3, 29) = 2.86$, $p = 0.054$ and 120 dpi (N = 7-8): $F(2, 19) = 6.24$, $p = 0.08$) and representative tracks of movement patterns of mice in an open field box are

presented. There was no significant difference between all tested groups. (C), (D) Activity percentage of mice in the periphery (One-way ANOVA - 30 dpi (N = 7-10): F (3, 29) = 2.15, p = 0.11 and 120 dpi (N = 7-8): F (2, 19) = 2.73, p = 0.09) and center part (One-way ANOVA - 30 dpi (N = 7-10): F (3, 29) = 2.14, p = 0.11 and 120 dpi (N = 7-8): F (2, 19) = 2.73, p = 0.09) of open field arena as well did not show any significant changes. Therefore, no sickness behavior, locomotors deficiency or anxiety-like behavior was detectable in infected mice. (E), (F) The percentage of time spent in the open (One-way ANOVA - 30 dpi (N = 7-10): F (3, 29) = 3.80, p = 0.20 and 120 dpi (N = 7-8): F (2, 19) = 1.00, p = 0.38) and closed arms (One-way ANOVA - 30 dpi (N = 7-10): F (3, 29) = 1.61, p = 0.20 and 120 dpi (N = 7-8): F (2, 19) = 0.18, p = 0.83) of elevated plus maze were similar in all groups tested at 30 and 120 days pi. Mice did not indicate elevated anxiety levels. Data are presented as mean ± SEM, ordinary one-way ANOVA of data and post hoc Bonferroni's multiple comparisons test were performed.

Figure 3. Long-term effect of influenza A virus infection on hippocampus-dependent spatial learning. (A) During 8 days of acquisition training, the escape latency reduced significantly in each group of control and infected mice, at 30 days pi the escape latency in H7N7 infected mice was significantly increased compared to control and non-neurotropic H1N1 and H3N2 IAV infected mice. (B) At 120 days pi the escape latency in all control, as well as IAV infected mice, did not reveal any significant differences. One single probe trial was performed after day 3, 6 and 9 of the training period. (C) The percentage of time spent in the target quadrant (NE) by H1N1 and H3N2 IAV infected mice at day 30 pi was increased similarly to control mice, whereas H7N7 infected mice showed a significantly reduce target quadrant preference on day 6 and 9 compared to the other groups tested. (D) The quadrant preference during the probe trials 120 days pi was similar in all groups. Data are presented as mean ± SEM (N = 7-10), one-way and two-way ANOVA of data and post hoc Bonferroni's multiple comparisons test were performed. * $p < 0.05$ and *** $p < 0.001$ compared to control. ++ $p < 0.01$ and +++ $p < 0.001$ compared to H1N1. ^ $p < 0.05$, ^^ $p < 0.01$ and ^^^ $p < 0.001$ compared to H3N2.

Figure 4. Analysis of learning strategies reveals a spatial learning impairment for both neurotropic and non-neurotropic virus subtypes. With regard to the different searching strategies to locate the hidden platform during the acquisition

phase of the Morris water maze experiment, hippocampus-independent searching strategies including random swimming, chaining and scanning decreased over time whereas the hippocampus-dependent strategy directed search increased. The searching strategies (directed search, chaining, scanning and random swimming) were color coded and the relative contribution of the respective strategy is presented for each day of the Morris water maze task. (A) The hippocampus-dependent strategy was decreased following H7N7 infection compared to the other groups, also H3N2 infected mice showed a reduction in the usage of direct search at 30 days pi. (B) No significant differences in searching strategies between IAV infected and control mice were observed 120 days pi. Data are presented as mean ± SEM (N = 7-10), two-way ANOVA of data and post hoc Bonferroni's multiple comparisons test were performed. * $p < 0.05$ and ** $p < 0.01$ compared to control. + $p < 0.05$ compared to H1N1.

Figure 5. Infection with neurotropic and non-neurotropic virus subtypes impairs memory formation for a new platform position. (A) During 3 days of training, the escape latency to a new position of the hidden platform (SW) decreased significantly in control, H1N1 and H7N7 influenza infected mice over days, however, not in H3N2 influenza infected mice. H7N7 IAV infected mice had a significantly elevated escape latency compared to control and H1N1 infected mice. (B) At 120 days pi, the IAV infected group did not show any significant differences in the escape latency compared to the control. A single probe trial test 24 hours after the last day of reversal training was performed. (C) Only control and H1N1 infected mice spent significantly more time in the new target quadrant (T) in comparison with the average time spent in non-target quadrants (NT). (D) All tested groups spent more time in T compared to NT 120 days pi. Data are presented as mean ± SEM (N = 7-10), in A and B repeated measure one-way and two-way ANOVA of data and post hoc Bonferroni's multiple comparisons test and in C and D unpaired t test were performed. ** $p < 0.01$ compared to control. + $p < 0.05$ and +++ $p < 0.001$ compared to H1N1. # $p < 0.05$, ## $p < 0.01$ and ### $p < 0.001$ compared to NT.

Figure 6. Long-term effect of influenza A virus infection on the function of CA1 hippocampal neurons. (A) input-output curves of field excitatory postsynaptic potential (fEPSP) slopes in hippocampal slices (n = 10) of control and infected mice at 30 days and 120 days pi did not show any significant differences between groups.

(B) Paired-pulse facilitation (PPF) of fEPSP slopes depicted as response to the 2nd stimulation over the 1st at different interpulse intervals (10, 20, 40, 60, 80, and 100 ms) in hippocampal slices (n = 9-11) did not show any differences between the groups at 30 and 120 days pi. (C) Hippocampal slices from H7N7 infected mice (n = 15) exhibited significantly lower induction and maintenance of LTP compared to control, whereas H3N2 infected mice (n = 13) showed a reduced maintenance of LTP compared to control (n = 17) at 30 days pi. (D) At the induction phase of LTP (T 20-25), only hippocampal slices from H7N7 infected mice had a significantly reduced LTP, however, at the stable phase of LTP (T 75-80) both groups of slices from H3N2 and H7N7 influenza virus infected mice revealed a significant reduction in LTP compared to control hippocampal slices. (E-F) At 120 days pi, the induction and maintenance phases of LTP did not show any differences in control and infected groups (n = 11-15). Data are presented as mean ± SEM (N = 4-5), in A and B, C and E two-way ANOVA of data and in D and F one-way ANOVA of data and post hoc Bonferroni's multiple comparisons test were performed. * $p < 0.05$ and ** $p < 0.01$ compared to control and ^ $p < 0.05$ compared to H3N2. N is number of mice and n is number of hippocampal slices in each group.

Figure 7. Long-term effect of influenza A virus infection on dendritic spine density of hippocampal neurons. (A) Representative images of Golgi-stained hippocampus sections (Scale bar = 200 µm, 2.5X), hippocampal neurons (Scale bar = 20 µm, 20X) and dendritic spines in hippocampal CA1-apical neurons following infection with influenza A viruses (Scale bar = 2 µm, 63X). (B-E) Following infection with H3N2 and H7N7 IAV, the spine density of apical dendrites of CA1 (B) and CA3 (C) hippocampal neurons decreased at 30 days pi, only H7N7 IAV infection reduced dendritic spine density of dentate granule cells located in the superior (D) and inferior blade (E) of the granule cell layer. Notably, 60 days pi a partial recovery occurred in the DG and CA3 hippocampal subregions of infected animals, and 120 days pi the dendritic spine density fully recovered in all regions of the hippocampus. Data are presented as mean ± SEM (N = 4-5 and number of dendrites in each group = 40-50), one-way ANOVA of data and post hoc Bonferroni's multiple comparisons test were performed. * $p < 0.05$ and *** $p < 0.001$ compared to control. ## $p < 0.01$ and ### $p < 0.001$ compared to 30 days pi time point.

Figure 8. Long-term effect of influenza A virus infection on glial cell density and activation status within the hippocampal subregions. (A) Representative examples of IBA-1 immunostaining at 30 days pi (Scale bar = 100 µm). Inserts: Higher magnifications of the respective images (Scale bar = 10 µm). (B) Following infection with H3N2 IAV, microglia density in the CA3 region and inferior blade of the dentate gyrus was increased significantly, whereas the neurotropic H7N7 IAV infection induced an increased microglia density in all hippocampal subregions at 30 days pi. Notably, 60 days pi a partial recovery occurred in the CA3 and DG regions of infected mice and 120 days pi microglia density was fully recovered in all subregions of the hippocampus (N = 4 and number of ROIs in each group = 20). The activation status of microglia was assessed by counting the number of primary processes. (C) Following infection with H3N2 and H7N7 IAV, the number of primary processes of microglia in all subregions of the hippocampus decreased at 30 days pi, however, upon H7N7 infection, the strongest reduction became visible in the superior and inferior blade of the granule cell layer. On the other hand, 60 days pi a partial recovery occurred in the CA3 and DG regions of infected mice, and 120 days pi microglia activation status was fully recovered in all subregions of the hippocampus (N = 4 and number of selected microglia in each group = 120-200). (D) Representative examples of GFAP immunostaining at 30 days pi (Scale bar = 50 µm). Inserts: Higher magnifications of the respective images (Scale bar = 10 µm). (E) Astrocyte density in all hippocampal subregions was increased at 30 days pi with H7N7 IAV, whereas only CA1 and CA3 were affected after H3N2 IAV infection. Interestingly, at 60 days pi and 120 days pi a reduction of GFAP positive cells to the level of controls was observed (N = 2-4 and number of ROIs in each group = 5-20). Data are presented as mean ± SEM, one-way ANOVA of data and post hoc Bonferroni's multiple comparisons test were performed. * $p < 0.05$ and *** $p < 0.001$ compared to control. ^^^ $p < 0.001$ compared to H3N2. # $p < 0.05$, ## $p < 0.01$ and ### $p < 0.001$ compared to 30 days pi time point.

Figure 9. Effect of influenza A virus infection on blood-brain barrier (BBB) permeability and cytokine level. (A) The injection of Evans blue dye for assessment of the BBB integrity upon infection with H3N2 and H7N7 IAV showed an increased Evans blue absorbance on day 8 post infection in both H3N2 and H7N7 infected mice (N = 3-4 and number of samples in each group = 6-8). (B) On day 10

post infection, Evans blue dye was well-visible macroscopically only in H7N7 infected mice, whereas in H3N2 infected mice it was only weakly visible around the ventricle (black arrow). (C-H) The levels of IFN-γ and TNF-α were significantly elevated in the blood serum, brain and hippocampus of H7N7 IAV infected mice. (H) H1N1 and H3N2 non-neurotropic IAV infection led to significantly increased TNF-α level within the hippocampus of infected mice (N = 2-4 and number of samples in each group = 3-8). Data are presented as mean ± SEM, one-way ANOVA of data and post hoc Bonferroni's multiple comparisons test were performed. * $p < 0.05$, ** $p < 0.01$ and *** $p < 0.001$ compared to control.

Figure 10. Whole genome microarray analysis from hippocampus of influenza infected mice at 18 and 30 days pi. DEPs (differentially expressed probesets) were identified based on an adjusted p-value of < 0.1 and exhibiting more than a 1.4 fold (log2 of 0.5) difference in expression levels. (A) At 18 days pi, 487 and 174 DEPs were detected in the hippocampus of H3N2 and H7N7 infected mice respectively. However, at 30 days pi, DEPs (250) were only found in H7N7 IAV infected mice. (B) Overlap of differentially expressed genes (DEGs) that are represented by the DEPs is presented as Venn diagram. (C) KEGG pathway analysis of DEGs following H3N2 and H7N7 IAV infection revealed significant pathways involved in local immune responses and cell adhesion molecules in the hippocampus of H3N2 and H7N7 infected mice at 18 days pi which are more pronounced and continued until 30 days pi for H7N7 IAV infection. The diameter of the dots indicates the gene ratio; range of 0.05 (smallest dot) to 0.20 (biggest dot), colors show significance of DEG representation for each pathway. (D) Relative changes (with reference to mock-infected mice) in expression levels of microglia signature and activation genes in the hippocampus after IAV infection. Data are presented as LogFC (fold change) mean in each groups compared to control group (N = 3-4 ad independent biological replicates). P-value is adjusted using Benjamini-Hochberg correction for multiple testing.

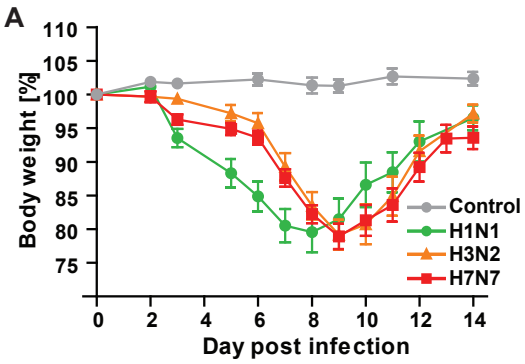

B

dpi	H1N1	H3N2	H7N7
3	nd	3/5	2/5
4	0/5	5/5	4/5
5	nd	3/5	5/5
7	0/4	5/5	4/4
9	nd	0/4	4/4
11	0/4	0/5	1/7

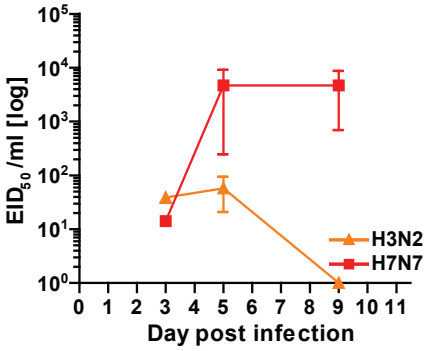

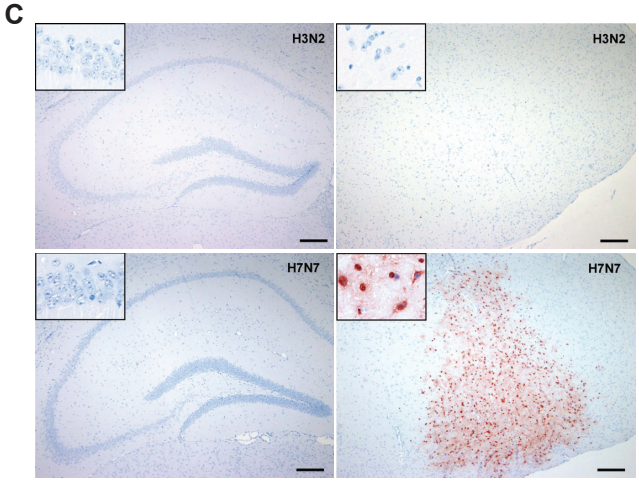

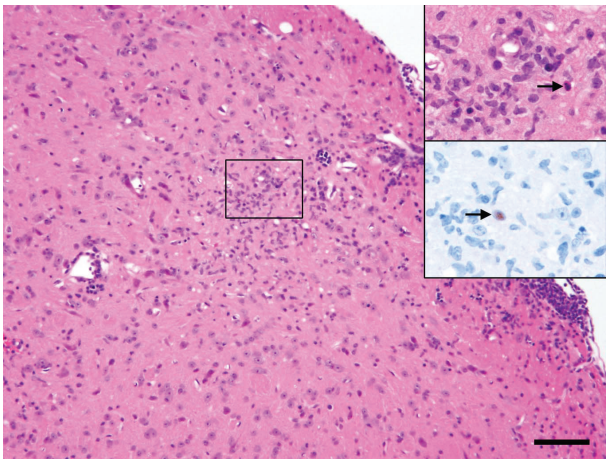

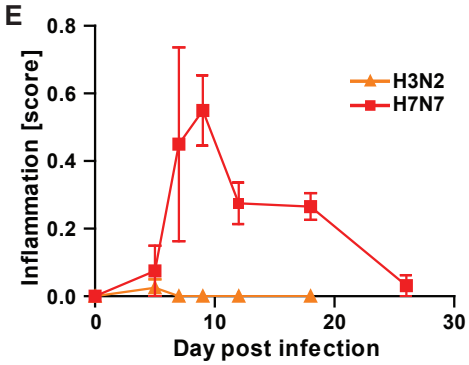

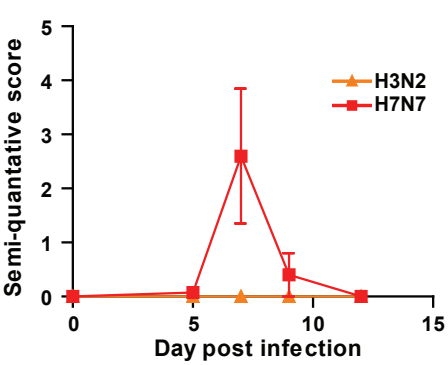

Figure 1. Hosseini et al.

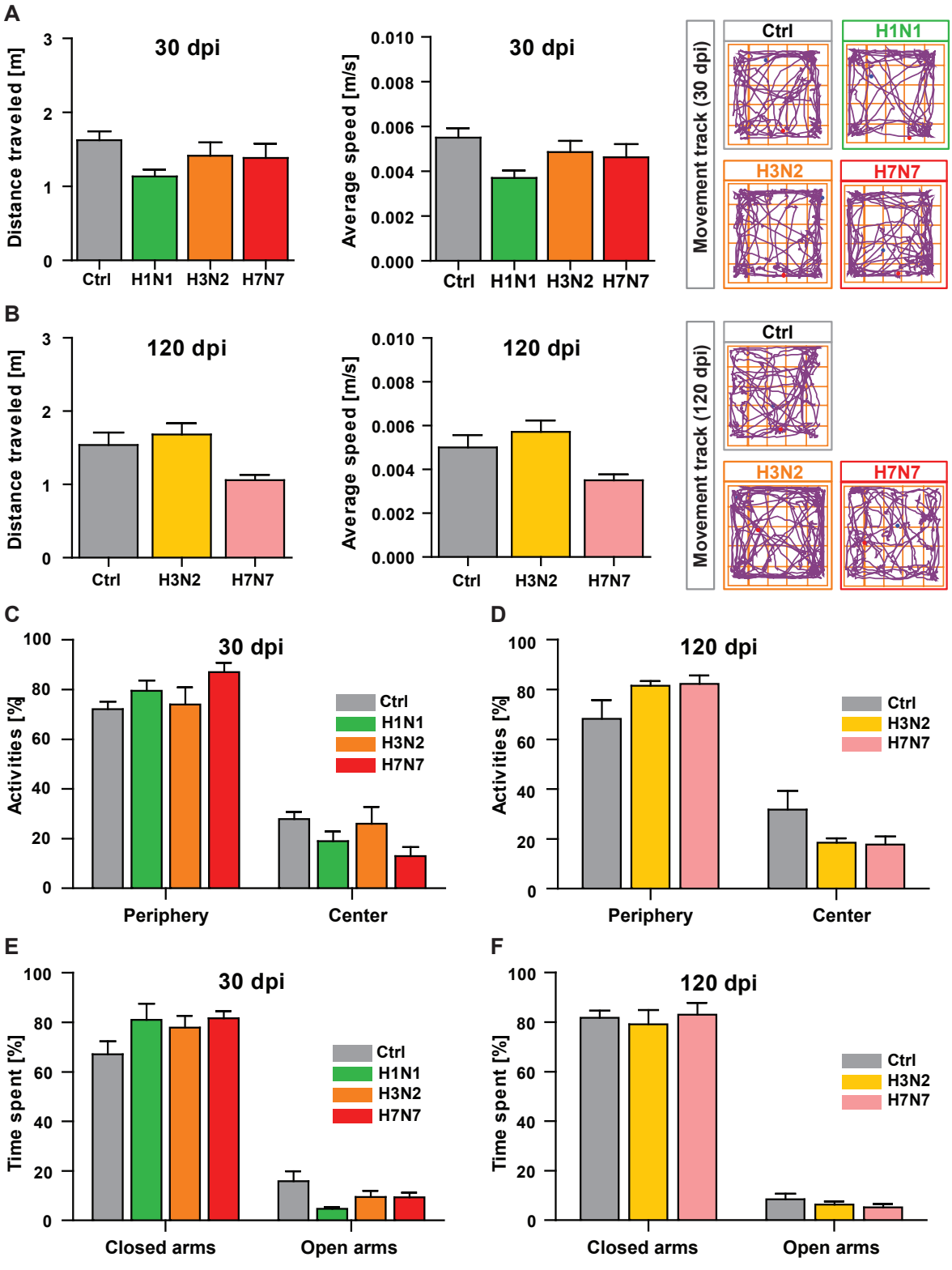

Figure 2. Hosseini et al.

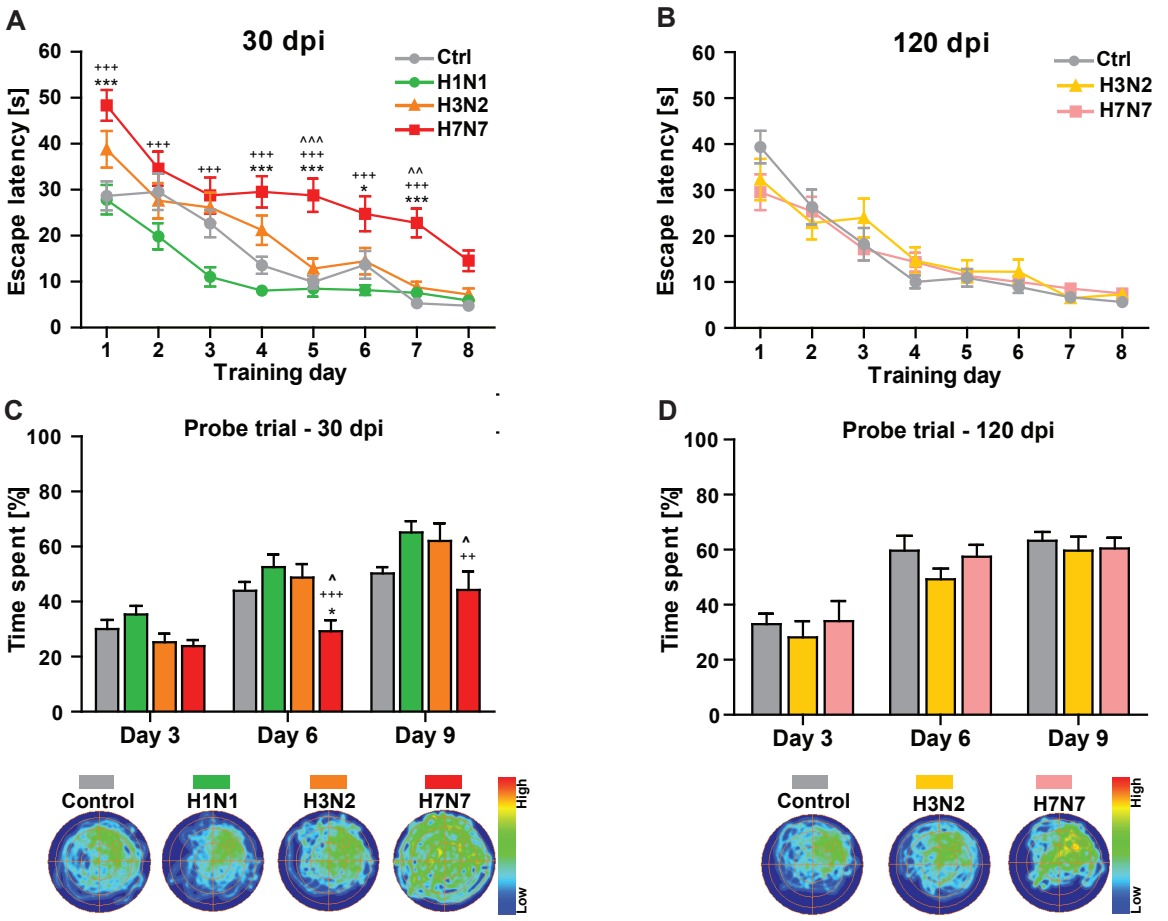

Figure 3. Hosseini et al.

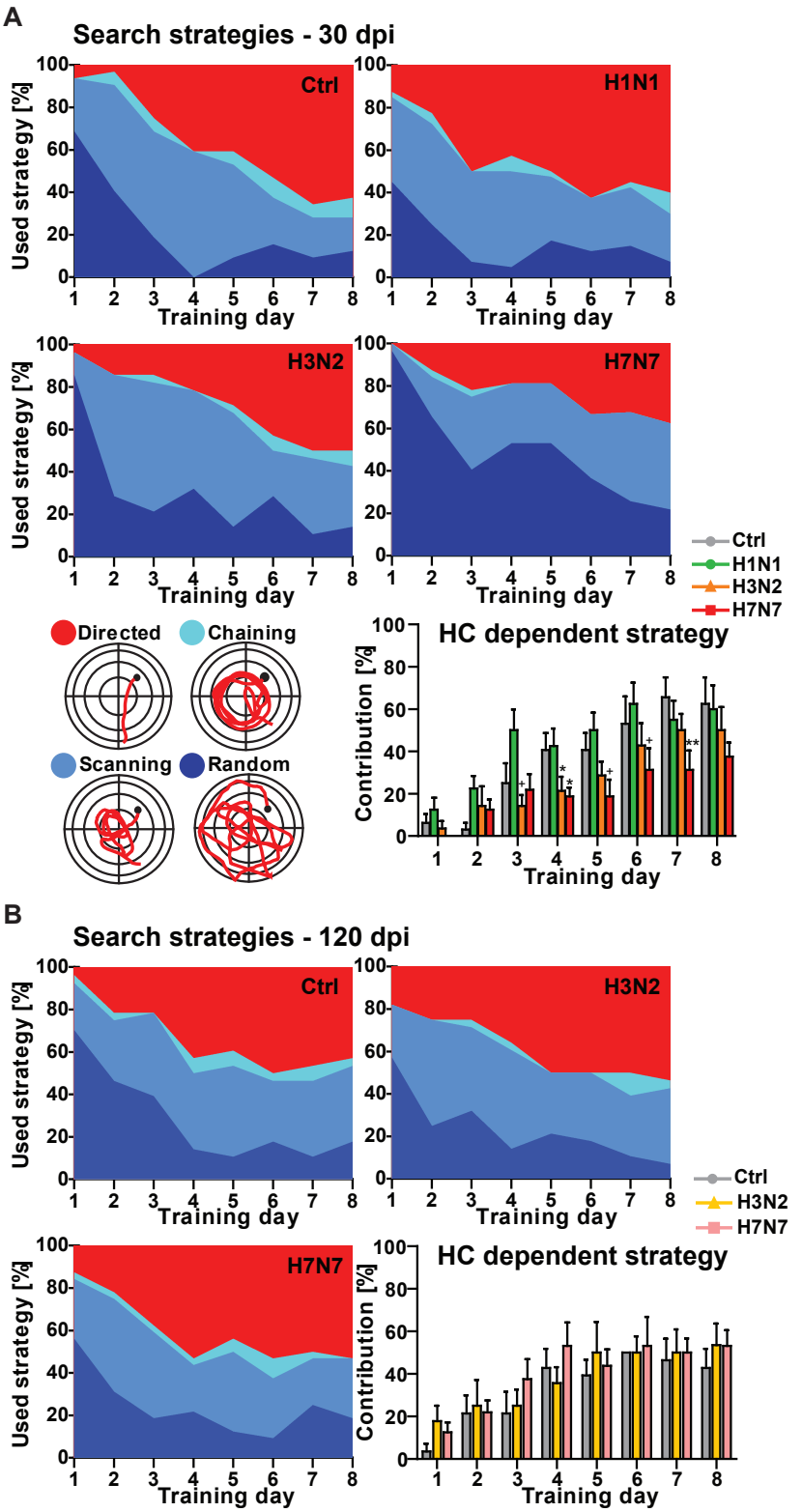

Figure 4. Hosseini et al.

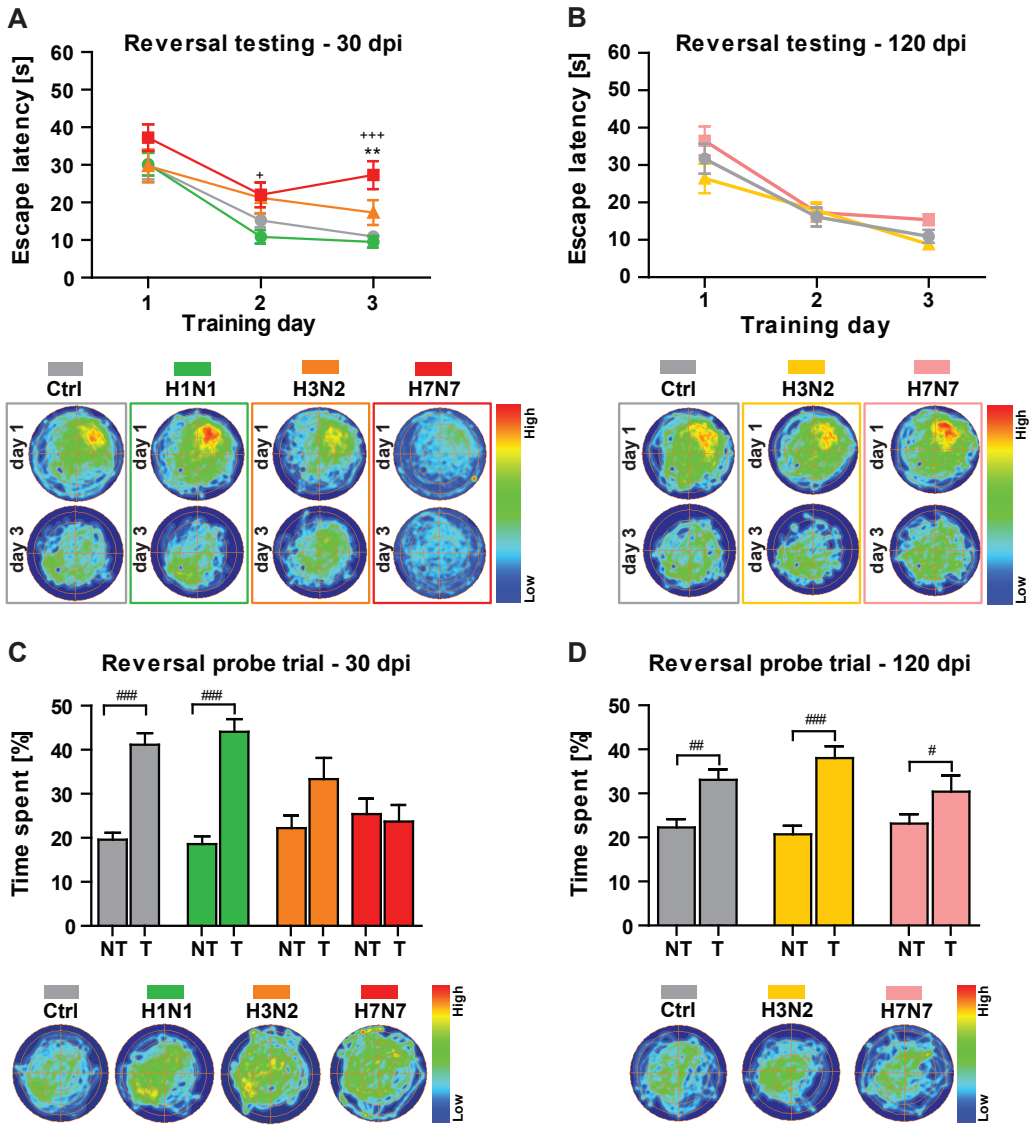

Figure 5. Hosseini et al.

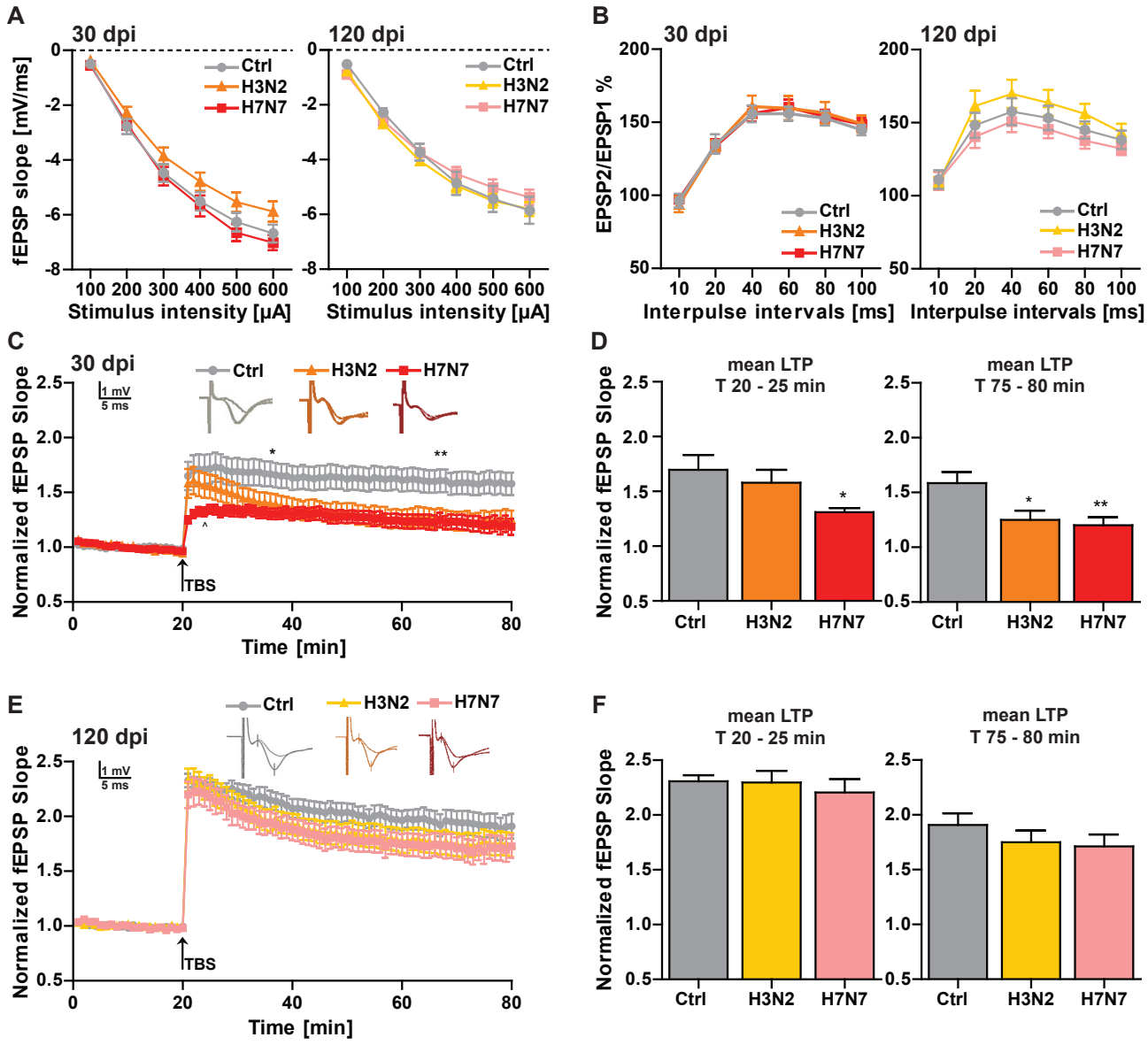

Figure 6. Hosseini et al.

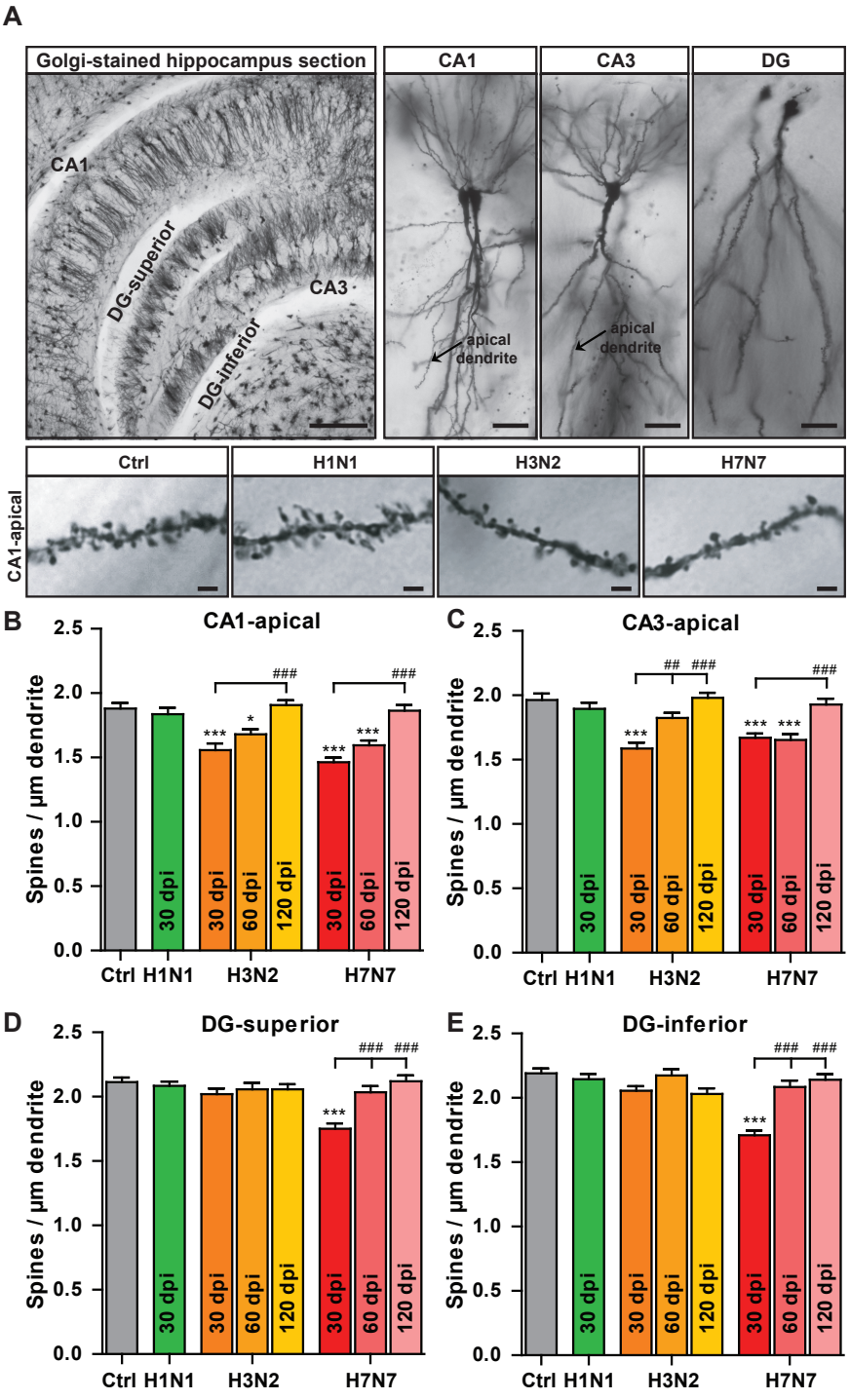

Figure 7. Hosseini et al.

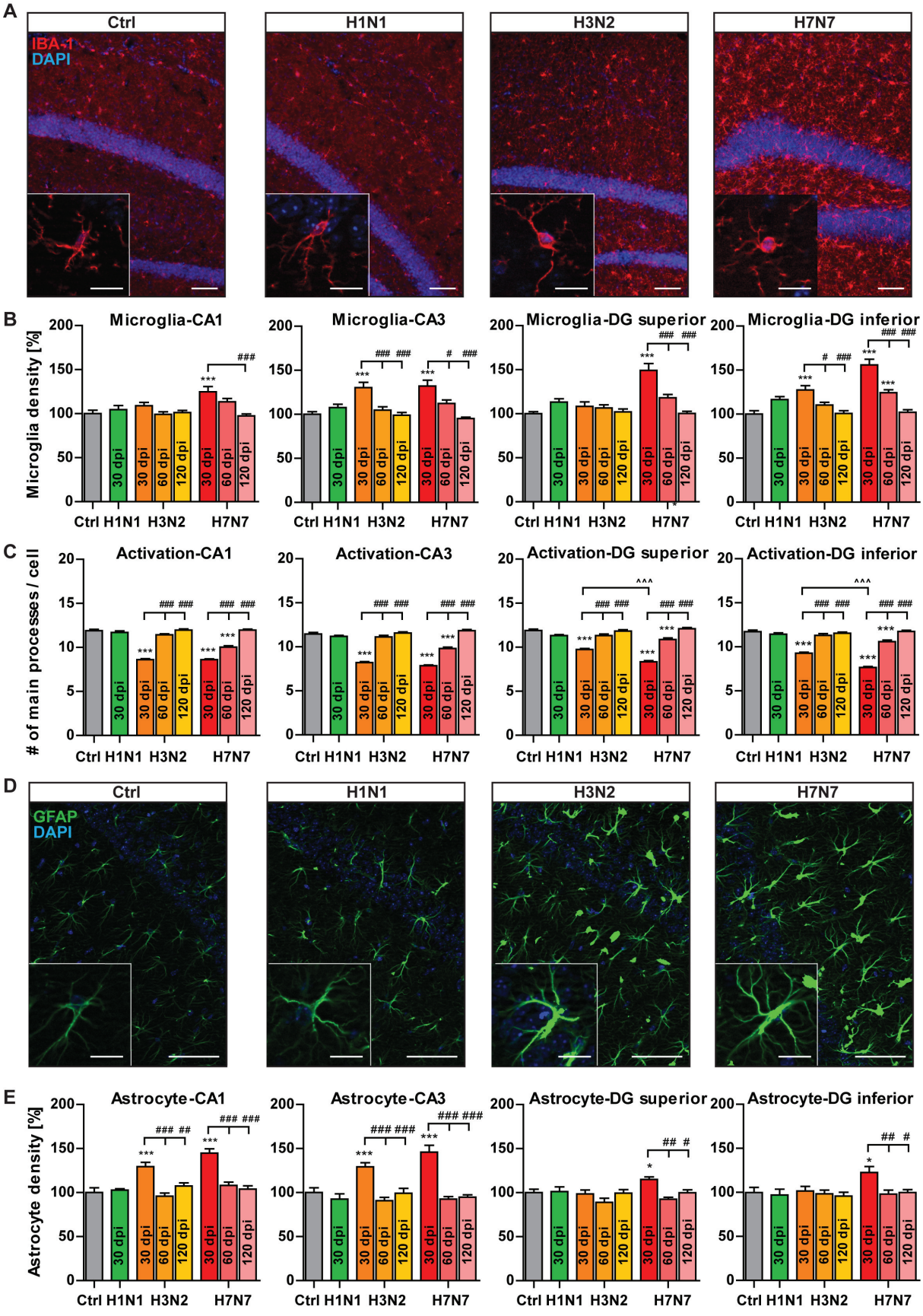

Figure 8. Hosseini et al.

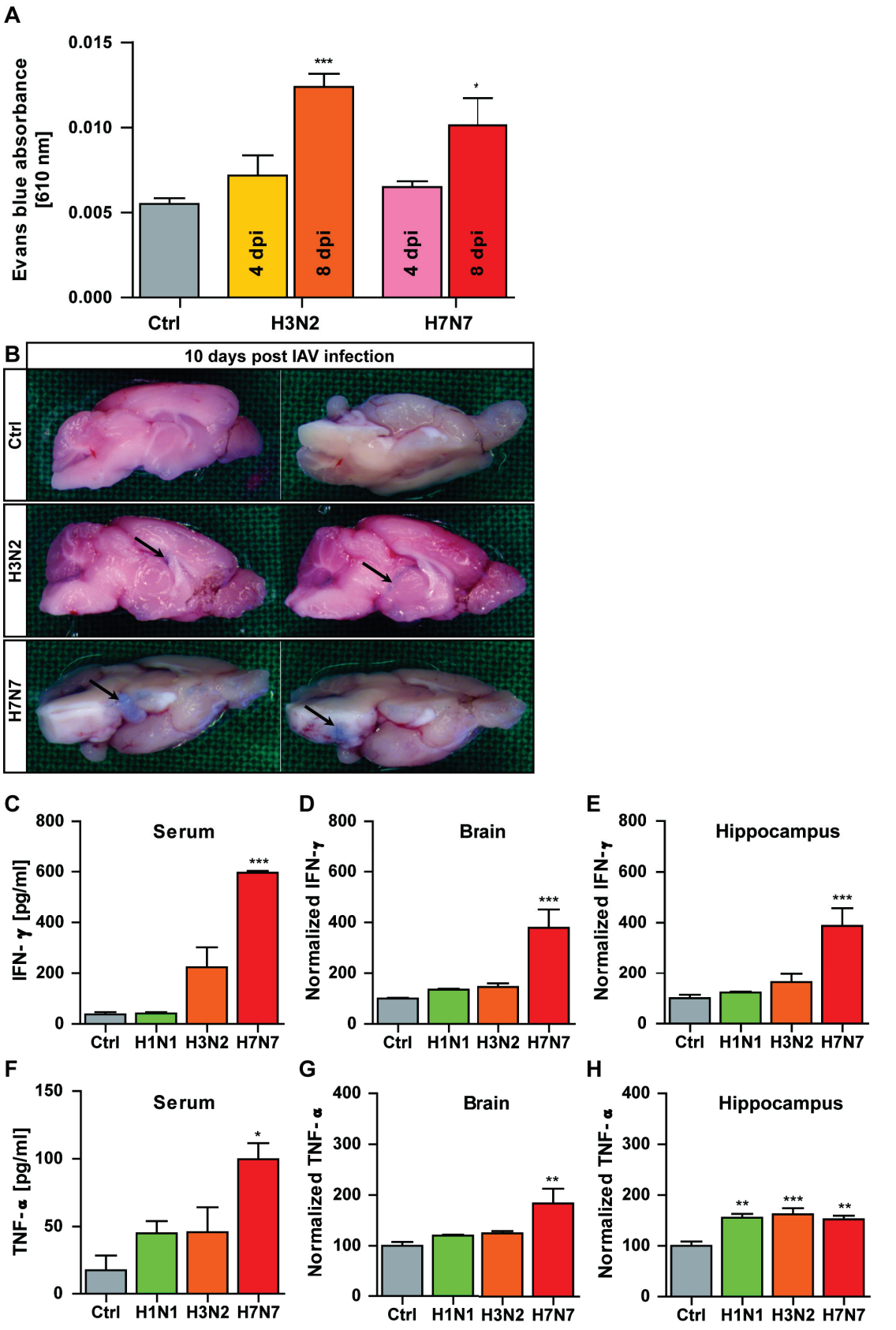

Figure 9. Hosseini et al.

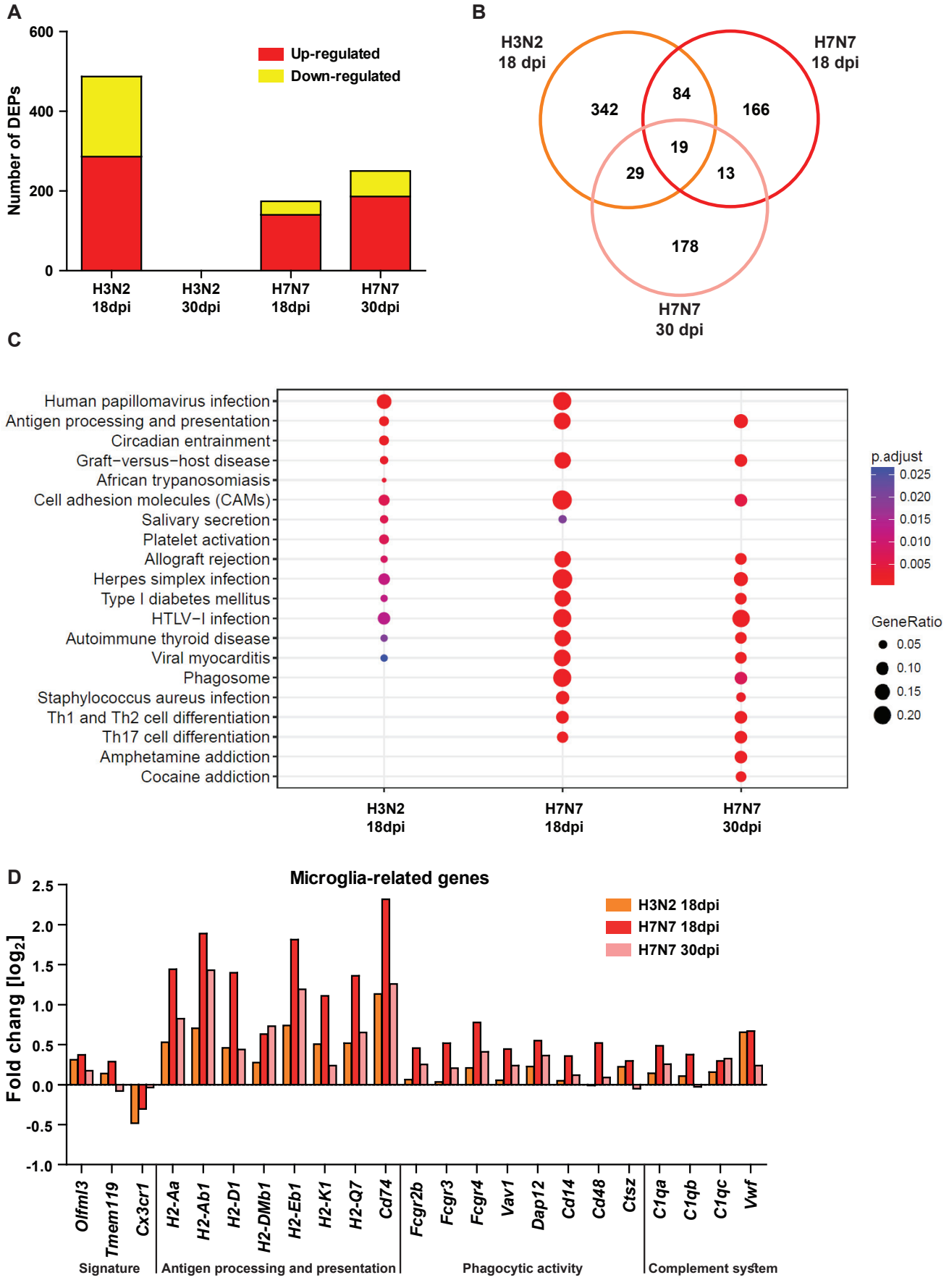

Figure 10. Hosseini et al.

	Symbol	Description	Function	Fold change [log_2]			Studies
				H3N2 18 dpi	H7N7 18 dpi	H7N7 30 dpi	
Neuron-related genes and neurotrophic factors	***Rbfox3***	RNA binding protein, fox-1 homolog (C. elegans) 3, (NeuN)	Marker of mature neurons, required for hippocampal circuit balance and function	**-0.461 ***	**-0.504 ***	**-0.223 ***	(Wang et al., 2015)
	Nrcam	neuronal cell adhesion molecule	Regulator of axon growth, schizophrenia and autism candidate gene	**-0.472 ***	**-0.431 ***	**-0.352 ***	(Demyanenko et al., 2014)
	Cacna1c	calcium channel, voltage-dependent, L type, alpha 1C subunit	Neuropsychiatric disease-associated gene, mediates survival of young hippocampal neurons	**-0.224 ***	**-0.390 ***	**-0.101**	(Lee et al., 2016)
	Dlg3	discs, large homolog 3 (Drosophila)	Synapse-associated protein 102, involved in spatial learning strategy and synaptic plasticity	**-0.356 ***	**-0.337 ***	**-0.206 ***	(Cuthbert, 2007)
	Grm5	glutamate receptor, metabotropic 5	Encodes mGluR5, decreased following viral infection	**-0.460 ***	**-0.320**	**0.096**	(Vasek et al., 2016)
	***Slc4a7* (NBCn1)**	solute carrier family 4, sodium bicarbonate cotransporter, member 7	Expressed in hippocampal neurons, associated with a Na^+ conductance, some NBCn1 colocalizes with the postsynaptic density marker PSD-95	**-0.494 ***	**-0.534 ***	**+0.123**	(Cooper et al., 2005; Majumdar and Bevensee, 2010)
	Slc6a3	solute carrier family 6 (neurotransmitter transporter, dopamine), member 3	Increased in depression and other psychiatric disorders	**+1.460**	**+3.160**	**+5.090 ***	(Uddin et al., 2011)
	Bdnf	brain derived neurotrophic factor	Required for support the survival of existing neurons, and encourage the growth and differentiation of new neurons and synapses	**-0.437 ***	**-0.515 ***	**-0.112**	(Huang and Reichardt, 2001)
	Ntf3	neurotrophin 3		**-0.580 ***	**-0.460 ***	**-0.110**	
Glia-related genes	***Gfap***	glial fibrillary acidic protein	Protein in the cytoskeleton of astrocytes, elevated level represents astroglial activation and gliosis during neurodegeneration	**+0.620 ***	**+0.476**	**+0.108**	(Brahmachari et al., 2006)
	Psmb8	proteasome (prosome, macropain) subunit, beta type 8 (large multifunctional peptidase 7)	Astrocytic immunoproteasome related gene, increased in Alzheimer's disease	**+0.200 ***	**+0.820 ***	**+0.390 ***	(Orre et al., 2013)
	Slc1a2	solute carrier family 1 (glial high affinity glutamate transporter), member 2 (EAAT2/GLT-1)	Associated gene with glutamate transport and metabolism, required for proper synaptic activity	**-0.492 ***	**-0.183**	**-0.185 ***	(David et al., 2009)
	Slc2a1	solute carrier family 2 (facilitated glucose transporter), member 1 (GLUT-1)	Responsible for glucose uptake into astrocytes and neurons, decreased in Alzheimer's disease	**-0.213 ***	**-0.311 ***	**+0.537 ***	(Liu et al., 2008)
	Slc30a5	solute carrier family 30 (zinc transporter), member 5	Zinc deficiencies lead to dementia, downregulated during aging and Alzheimer's disease	**-0.331 ***	**-0.240 ***	**+0.037**	(Lovell, 2009; Nuttall and Oteiza, 2014; Crotti and Ransohoff, 2016)
Interferon-response gene	***Psmb9 (LMP2)***	proteasome (prosome, macropain) subunit, beta type 9 (large multifunctional peptidase 2)	IFN-α-inducible gene, depression-associated gene	**+0.221 ***	**+0.790 ***	**+0.516 ***	(Hoyo-Becerra et al., 2015)
	Lgals3bp	lectin, galactoside-binding, soluble, 3 binding protein	Type I IFN-induced gene, modulation activity of immune cells	**+0.415 ***	**+0.674 ***	**+0.441 ***	(Goffinet, 2016)
	Oas2	2'-5' oligoadenylate synthetase 2	Involved in defense and innate immune response to virus	**+0.431 ***	**+0.759 ***	**+0.492 ***	(Bao et al., 2017)
	Ccl5	chemokine (C-C motif) ligand 5	Type I IFN-induced chemokine, associated with hippocampal T-cell infiltration, promotes cognitive decline	**+0.408 ***	**+2.150 ***	**+1.523 ***	(Laurent et al., 2017)
	Ifit3	interferon-induced protein with tetratricopeptide repeats 3	Stat1 and IFN signaling-dependent gene, expression higher in granule cell neurons	**+0.084**	**+0.690 ***	**+0.201**	(Cho et al., 2013)

Table 1. Relative changes in expression levels of candidate genes in the hippocampus of IAV infected mice

Significant regulation (* $p < 0.1$, BH adjusted) is marked with an asterisk. A partial recovery in the altered genes expression was observed 30 days post H7N7 infection.

Table 1. Hosseini et al.